Contributions to Mineralogy and Petrology (2019) 174:19
https://doi.org/10.1007/s00410-019-1552-z

ORIGINAL PAPER

Subduction relics in the subcontinental lithospheric mantle evidence from variation in the $\delta^{18}O$ value of eclogite xenoliths from the Kaapvaal craton

Ioana-Bogdana Radu[1,2] · Chris Harris[1] · Bertrand N. Moine[2] · Gelu Costin[3] · Jean-Yves Cottin[2]

Received: 14 October 2018 / Accepted: 31 January 2019 / Published online: 26 February 2019

Abstract

Mantle eclogites are commonly accepted as evidence for ancient altered subducted oceanic crust preserved in the subcontinental lithospheric mantle (SCLM), yet the mechanism and extent of crustal recycling in the Archaean remains poorly constrained. In this study, we focus on the petrological and geochemical characteristics of 58 eclogite xenoliths from the Roberts Victor and Jagersfontein kimberlites, South Africa. Non-metasomatized samples preserved in the cratonic root have variable textures and comprise bimineralic (garnet (gt)–omphacite (cpx)), as well as kyanite (ky)- and corundum (cor)-bearing eclogites. The bimineralic samples were derived from a high-Mg variety, corresponding to depths of ~ 100–180 km, and a low-Mg variety corresponding to depths of ~ 180–250 km. The high-Al (ky-, cor-bearing) eclogites originated from the lowermost part of the cratonic root, and have the lowest REE abundances, and the most pronounced positive Eu and Sr anomalies. On the basis of the strong positive correlation between gt and cpx $\delta^{18}O$ values ($r^2 = 0.98$), we argue that $\delta^{18}O$ values are unaffected by mantle processes or exhumation. The cpx and gt are in oxygen isotope equilibrium over a wide range in $\delta^{18}O$ values (e.g., 1.1–7.6‰ in garnet) with a bi-modal distribution (peaks at ~ 3.6 and ~ 6.4‰) with respect to mantle garnet values (5.1 ± 0.3‰). Reconstructed whole-rock major and trace element compositions (e.g., MgO variation with respect to Mg#, Al_2O_3, LREE/HREE) of bimineralic eclogites are consistent with their protolith being oceanic crust that crystallized from a picritic liquid, marked by variable degrees of partial melt extraction. Kyanite and corundum-bearing eclogites, however, have compositions consistent with a gabbroic and pyroxene-dominated protolith, respectively. The wide range in reconstructed whole-rock $\delta^{18}O$ values is consistent with a broadly picritic to pyroxene-rich cumulative sequence of depleted oceanic crust, which underwent hydrothermal alteration at variable temperatures. The range in $\delta^{18}O$ values extends significantly lower than that of present day oceanic crust and Cretaceous ophiolites, and this might be due to a combination of lower $\delta^{18}O$ values of seawater in the Archaean or a higher temperature of seawater–oceanic crust interaction.

Keywords Eclogite xenoliths · Subcontinental lithospheric mantle · $\delta^{18}O$ · Subduction relics

Communicated by Jochen Hoefs.

Electronic supplementary material The online version of this article (https://doi.org/10.1007/s00410-019-1552-z) contains supplementary material, which is available to authorized users.

✉ Ioana-Bogdana Radu
ioanabogdana.radu@gmail.com

[1] Department of Geological Sciences, University of Cape Town, Private Bag X3, Rondebosch 7701, South Africa

[2] UJM Saint-Etienne, UCA, CNRS, IRD, Laboratoire Magmas et Volcans, UMR 6524, Université de Lyon, 42023 Saint-Étienne, France

[3] Department of Earth, Environmental and Planetary Sciences, Rice University, Houston, TX 77005, USA

Introduction

Evidence for the early evolution of the ancient oceanic crust is presumed to be preserved in deep continental roots (Aulbach et al. 2016; Jacob 2004). However, these are not directly accessible and their study is limited to xenoliths exhumed by kimberlite magmas. Although eclogite xenoliths are extremely rare, being < 1% of mantle xenoliths in kimberlites (Schulze et al. 2000) they may be the only relics of the ancient crust (Beard et al. 1996; Jacob and Foley 1999; Schulze and Helmstaedt 1988). The roots of most cratons contain scattered eclogite bodies, sometimes associated with diamonds, possibly concentrated around 120–150 km depth (Garber et al. 2018; Jacob 2004; Pearson 1999). Determining the origin of mantle

eclogites is key to understand the formation and thickening of stable continental domains (Aulbach 2012; Jacob 2004; Pearson 1999). Prior to or during their entrapment, most mantle xenoliths underwent kimberlitic/carbonatitic metasomatism that changed their primary composition (Howarth et al. 2014; Huang et al. 2012; Misra et al. 2004). This must be taken into account before any protolith can be reliably identified.

Several hypotheses have been proposed for the origin of mantle eclogites and their preservation in the cratonic root: (1) mantle-derived high-pressure cumulates (Caporuscio and Smyth 1990; Harte and Gurney 1975; Hatton 1978; Hatton and Gurney 1977; Lappin 1978; Lappin and Dawson 1975; MacGregor and Carter 1970; O'Hara and Yoder 1967; Smyth and Caporuscio 1984; Smyth et al. 1989); (2) metamorphosed fragments of a subducted oceanic crust (Agashev et al. 2018; Aulbach et al. 2016; Barth et al. 2002; Beard et al. 1996; Helmstaedt and Doig 1975; Jacob 2004; Jacob and Foley 1999; Jacob et al. 1994; MacGregor and Manton 1986; Radu et al. 2017; Riches et al. 2016a; Schulze and Helmstaedt 1988; Schulze et al. 2000; Shervais et al. 1988; Shu et al. 2016; Viljoen et al. 2005; Withers et al. 1998); and (3) subduction-derived melt residues (Barth et al. 2001; Ireland et al. 1994; Rollinson 1997; Shchipansky 2012; Snyder et al. 1993).

The high-pressure cumulate model fails to account for $\delta^{18}O$ values outside the 'normal' mantle range ($+5.5 \pm 0.4‰$ Mattey et al. 1994), the presence of a parental basaltic melt deeper than 200 km, the absence of ubiquitous olivine (Jacob 2004), or the excess silica and aluminium to produce kyanite for the entire range of bulk Mg# (Ater et al. 1984). Moreover, this model is most commonly based on grosspydite xenoliths, misclassified as eclogites (Harte and Gurney 1975; Lappin 1978; MacGregor and Carter 1970; O'Hara and Yoder 1967; Smyth et al. 1989).

Although seemingly more robust, the two crustal models (2, 3) have been in turn contested (Gréau et al. 2011; Griffin and O'Reilly 2007; Huang et al. 2014), and redox conditions have been proposed as alternative mechanisms that could have generated the recorded positive Eu, while Sr anomalies and $\delta^{18}O$ values higher than mantle ($>5.5‰$) have been attributed to mantle metasomatism. However, these alternative explanations do not account for eclogites with such a wide range in $\delta^{18}O$ values, and little consensus has been reached regarding the petrogenesis of mantle eclogites (Aulbach and Jacob 2016; Griffin and O'Reilly 2007; Huang et al. 2016; Radu et al. 2017).

Geological background

The Kaapvaal Craton broadly covers the centre of southern Africa, and is delimited by the Limpopo belt (~2.7 Ga) to the north, the Namaqua-Natal Province mobile belt (~1.1–1.9 Ga) to the south and east and by the overthrusted Kheis belt (~2.0 Ga) to the west (van Reenen et al. 1992). It generally stabilized between 3.7 and 2.6 Ga (de Wit et al. 1992), followed by a later disruption of the north-central part of the craton by the major intracrustal intrusion of the Bushveld Igneous Complex (James et al. 2003) at ~2.06 Ga. Seismic investigation shows a thin continental crust, with an intermediate to felsic composition at the base and a sharp, almost flat Moho (Schmitz and Bowring 2003), attributed to intensive re-melting of the lower crust, possibly related to the Ventersdorp extensional tectonics and magmatism (2.7 Ga). This is further supported by coeval granulite xenoliths, which have been interpreted as evidence for ultrahigh-temperature metamorphism (in excess of ~1000 °C in the lowermost crust) that may have affected the western and central part of the craton, including the Kimberley area (Schmitz and Bowring 2003). Partial melting and deep crustal ductile flow may have led to differentiation at the base of the crust and high-pressure–temperature (HP-HT) crystallization (James et al. 2003).

The Roberts Victor Mine (28°29′ S–25°33′ E) is located ca. 95 km northeast of Kimberley, in the centre of the Kaapvaal Craton (Fig. 1). It consists of two small Group-2 kimberlite pipes intruded at ca. 128 Ma (Smith et al. 1985), containing phenocrysts of olivine, diopside, spinel, perovskite and apatite, in a phlogopite-dominated groundmass, characterized by fine-grained textures; with elevated contents of SiO_2, K_2O, Pb, Rb, Ba and LREE-enriched composition (Field et al. 2008). The xenolith suite comprises Beaufort Group sandstone and Karoo basalt from the overlying strata, but is mostly dominated by mantle eclogites (>95%), as well as xenocrysts and severely altered peridotites, often diamond-bearing (Hatton 1978). Eclogite xenoliths interpreted to have retained the age of their formation have been previously dated at 1.7 Ga (Jagoutz et al. 1984), 1.4–2.2 Ga (Jacob et al. 2005), 0.7–1.1 Ga and 1.2–1.5 Ga (Huang et al. 2012) and 0.9–1.9 Ga (Gonzaga et al. 2010).

The Jagersfontein Mine (29°46′ S–25°25′ E) is located ca. 170 km southeast of Kimberly, close to the craton margin. It is one of the large Group-1 kimberlite pipes, dated at ~85 Ma (Smith et al. 1985), containing olivine, monticellite, calcite, phlogopite, ilmenite, spinel, perovskite and apatite in a micaceous groundmass (Field et al. 2008), with a relatively coarse-grained texture. The xenolith suite includes peridotites, eclogites, pyroxenites and megacrysts. Two main metasomatic imprints (hydrous and carbonate) have been described for the eclogite suite (Pyle and Haggerty 1998). Both peridotitic and eclogitic inclusions have been found contained within diamonds (Field et al. 2008). Some xenoliths exhibiting omphacite exsolution in garnet have been interpreted as being sourced from the upper Transition Zone limit (Haggerty and Sautter 1990). The only age constraints for eclogite formation are inferred from sulphide inclusions

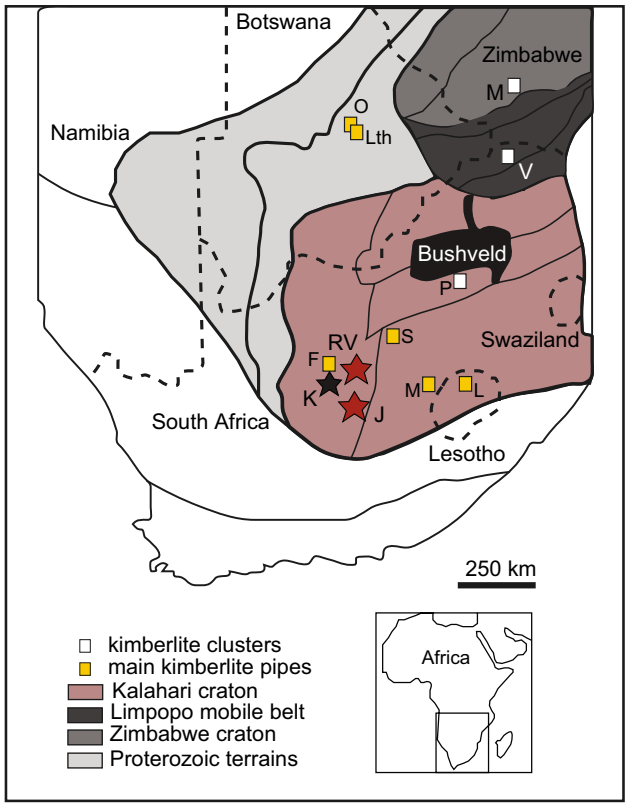

Fig. 1 Map of the Kalahari craton and separate terrains including the Kaapvaal and Zimbabwe cratons and the Limpopo Mobile Belt. *K* Kimberly cluster, *P* Premier/Cullinan cluster, *M* Murowa/Sese kimberlite, *V* Venetia kimberlite cluster, *RV* Roberts Victor mine, *F* Finsch, *J* Jagersfontein mine, *S* Star, *L* Letseng, *M* Monastery, *O* Orapa, *Lth* Letlhakane. After Van der Meer et al. (2013) and Katayama et al. (2009)

in diamonds (1.1–1.7 Ga), and the strongly radiogenic $^{187}Os/^{188}Os$ has been interpreted as possible indicator for an ancient, remobilized eclogitic source (Aulbach et al. 2009).

Petrography

The primary mineralogy of the eclogite xenoliths analyzed in this paper consists of a high-grade mineral assemblage of garnet (gt) and omphacitic clinopyroxene (cpx). Most are bimineralic, with rutile (ru) as the main accessory phase. Less frequently, they may contain coesite (typically found inverted to palisade quartz), diamond, graphite, kyanite (ky) and corundum (cor) as primary minor phases. They have variable grain size, grain boundaries, as well as modal abundance and colour. A few samples show exsolution textures such as topotactic (crystallographically controlled) lamellae or lenses of garnet and/or kyanite in clinopyroxene, or needle-like rutile in both omphacite and garnet. Samples showing interactions with kimberlitic/carbonaceous fluids typically contain secondary phlogopite, plagioclase feldspar and/or sanidine. Textures and mineral assemblages for each sample are summarized in Appendix A in the electronic supplementary material.

Bimineralic eclogites

Bimineralic eclogites range in size from a few centimetres (Jagersfontein) up to > 20 cm in diameter (Roberts Victor) and consist of omphacite and garnet, and are characterized by two main textural types: described as metasomatized and non-metasomatized by MacGregor and Carter (1970) and Huang et al. (2012). The former is the most common (Type I Gréau et al. 2011; MacGregor and Carter 1970), and is defined by subhedral to rounded, or "cauliflower"-shaped garnet grains, with serrated grain boundaries (Fig. 2a, b), underlined by a finely crystallized, seemingly opaque, secondary rim. Garnet can be found as grain clusters, 'necklaces' and less as isolated grains, marked by irregular intracrystalline fine fractures associated with scattered glass and melt inclusions that give an overall 'dusty' appearance. Garnet ranges in size and modal abundance, with colour from dark to pale orange but showing no textural zoning. Omphacite is present as inequigranular, sub- to anhedral grains, often with destabilized symplectic rims and with poorly preserved cores (Fig. 2a, b). The xenomorphous crystals are highly altered along irregular fractures by carbonate-rich fluids and form an interstitial matrix around garnet. The colour of omphacite varies from dark to light green (in plane polarized light), with irregular grain boundaries doubled by symplectic plagioclase, diopside and fine-grained phlogopite. Rutile is interstitial and texturally bound to the fine-grained secondary minerals.

Non-metasomatized eclogites (defined as Type II Gréau et al. 2011; MacGregor and Carter 1970) are less common than Type I, and are characterized by sub- to anhedral garnet, which is less fractured and more systematically coarse grained, and bordered by a fine opaque rim (Fig. 2c, d). The colour of the garnet varies from dark to pale orange. A few samples have fine, elongated anhedral garnet bordering clinopyroxene. Omphacite occurs as a sub- to anhedral, inequigranular matrix. Its colour ranges from dark to pale green, with well-preserved translucent cores, often surrounded by symplectic (diopside-plagioclase) rims of variable thickness. Often, rutile is found as needle-like exsolution spread throughout both garnet and omphacite.

High-Al eclogites

High-Al eclogites contain mineral phases such as kyanite and corundum. Kyanite-bearing xenoliths are characterized by sub- to anhedral, inequigranular garnets with straight to slightly indented grain boundaries (Fig. 2e), ranging from

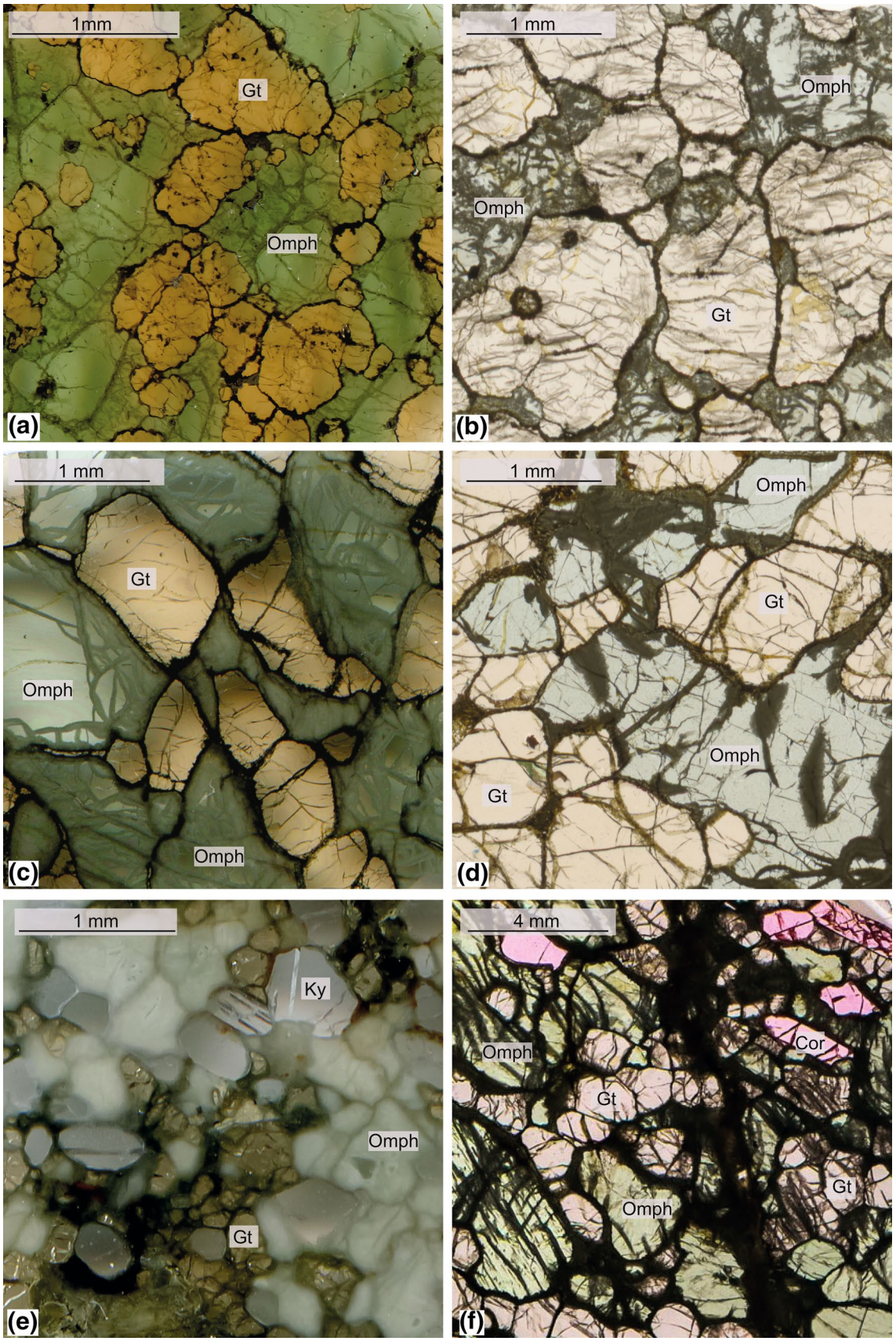
1mm
Gt
Omph
(a)
1 mm
Omph
Omph
Gt
(b)
1 mm
Gt
Omph
Omph
(c)
1 mm
Omph
Gt
Omph
Gt
(d)
1 mm
Ky
Omph
Gt
(e)
4 mm
Omph
Cor
Gt
Gt
Omph
(f)

◂**Fig. 2** Scanned thin sections of representative Type I (**a, b**), Type II (**c–f**) (MacGregor and Carter 1970) bimineralic, kyanite- (**e**) and corundum-bearing (**f**) eclogites from Roberts Victor (**a, c, e, f**) and Jagersfontein (**b, d**) mines

light to dark brown in colour. Omphacite is broken down into a white "spongy" clinopyroxene matrix, sometimes with preserved translucent green cores and xenoblastic grain boundaries. Kyanite is found as small (30–40 µm), subhedral to tabular or rounded, isolated or clustered grains. Microcrystalline, opaque rims surround grain boundaries.

Omphacite is the dominant mineral (~ 60 vol%) in corundum-bearing eclogites, ranging from small (~ 0.3 cm) rounded grains, to large (~ 2 cm) subhedral light green crystals (Fig. 2f). Garnet is found as subhedral and rounded inequigranular grains, with straight grain boundaries and of typically light brown colour. The modal abundance of corundum varies from ~ 2–17 vol% and is found as pale to intense pink, subhedral to anhedral crystals. Often corundum grains are surrounded by garnet or kyanite-garnet coronae. Rutile is scarce, mostly interstitial.

Three types of exsolution texture are present (Fig. 3): fine oriented lamellae, coronae and granular clusters. The topotaxial lamellae (~ 50–300 µm) consist of garnet or kyanite bordered by garnet. Some samples exhibit crosscutting garnet lamellae in-between the host omphacite cleavage planes (Fig. 3a). There is continuity between the lamellae and corona textures, as lamellae can be found blending into the coarse coronae. The corona around corundum grains can be monophasic—consisting exclusively of garnet, or polyphasic—consisting of kyanite and garnet (Fig. 3b). The granular clusters consist of rounded, fine-grained (~ 0.1 mm) garnet grains.

Analytical techniques

Mineral (major element) compositions were acquired using a JEOL JXA-8320 electron microprobe at the Geology Department, Rhodes University, South Africa, equipped with four WDS, one FCS and two L-Type spectrometers and 12 diffraction crystals and at the Laboratoire Magmas et Volcans, Cézeaux, France, using a Cameca SX-100 electron microprobe, equipped with four WDS spectrometers and 12 diffraction crystals. Operating conditions were 15 keV and a beam current of 10 nA. The counting time was of 20 s for all elements, except K and Na (60 s), and 10 s for background. All data were processed using full ZAF Cameca PAP corrections.

Trace element compositions were acquired by laser ablation inductively coupled plasma spectrometry at the Laboratoire Magmas et Volcans, Cézeaux, France, using a Resonetics Resolution M-50 laser powered by an ultra-short pulse ATL AtlexExcimer laser system, beam diameter of 100 µm, 8 Hz repetition rate and 6 mJ laser pulse energy (detailed description in Müller et al. 2009). Reproducibility and accuracy of the analyses were estimated through repeated analyses of BCR-2g standard at the beginning and at the end of every run. Data reduction was carried out with the software package GLITTER® (Macquarie Research Ltd, 2001) (van Achterbergh et al. 2001). For each analysis, the time resolved signal for each element was monitored to discard perturbations related to inclusions, fractures or mixing.

Whole-rock compositions have been calculated based on individual mineral analyses and estimated modal abundance. Mineral proportions were determined on thin section scans and compositional maps (~ 10–20% uncertainty due to variable grain size and distribution), based on colour contrast between the different phases with the use of the Adobe®Photoshop® image-editing software. The errors in surface to volumetric conversions are negligible because the minerals concerned have similar densities and there is no preferred orientation of grains or layering in the rock.

The O isotope analyses were performed at the Department of Geological Sciences, University of Cape Town (UCT), South Africa, by the laser fluorination method described by Harris and Vogeli (2010). Mineral separates showed no optical evidence for alteration, fractures or inclusions. Duplicate and triplicate grain batches were analyzed for 15 out of a total of 36 samples and were reproducible within 0.67‰, and one of the samples with particularly low mineral $\delta^{18}O$ values has been analyzed up to 4 times the garnet, with a maximum difference of 0.17‰. Between 2.5 and 3.0 mg of each mineral (~ 4 grains in average) were reacted in the presence of ~ 10 kPa of BrF_5. The O_2 produced was collected onto molecular sieve at liquid nitrogen temperatures. Oxygen isotope ratios were measured off-line using a Finnigan DeltaXP mass spectrometer, in dual inlet mode, on O_2 gas. All values are reported relative to the SMOW scale, as $\delta = [(^{18}O/^{16}O)\ \text{sample}/(^{18}O/^{16}O)\ \text{standard} - 1] \times 1000$. The long-term average difference between duplicates of the in-house MONGT standard is 0.12‰ ($n = 283$), which corresponds to a 1σ error of 0.077.

Mineral chemistry

Worldwide, bimineralic eclogites that were metasomatized by fluids preceding the kimberlite magma (Type I) are characterized by alkali, LREE, Ba, Sr, and HFSE enrichment and are defined by ≥ 0.8 wt% K_2O in clinopyroxene and/or ≥ 0.9 wt% Na_2O in garnet (Gréau et al. 2011; Huang et al. 2012). Conversely, non-metasomatized eclogites (Type II) have alkali contents that are lower (Huang et al. 2012; McCandless and Gurney 1989) and are poor in LREE and LILE. Similarly, eclogite xenoliths have been divided into group

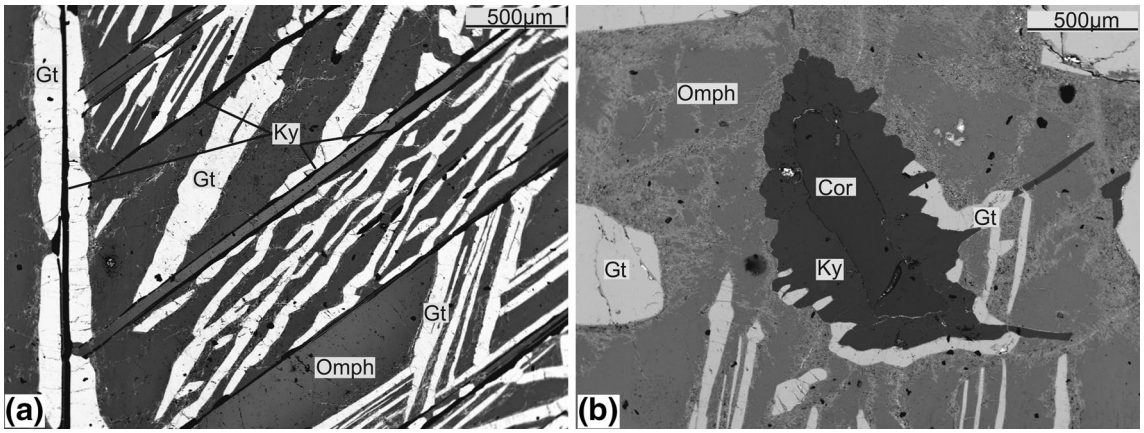

Fig. 3 BSE images of representative exsolution textures in corundum-bearing eclogites from Roberts Victor. Large omphacite grains exhibit topotaxial garnet, garnet and kyanite exsolution lamellae (**a**). Some samples contain crosscutting garnet lamellae in-between the cleavage planes. Corundum grains are often surrounded by monophasic (garnet) or polyphasic (kyanite and garnet) coronae (**b**)

A (Mg-rich), group B and group C (with increasing jadeite and grossular contents) based on the Ca–Mg ratio in garnet and Na content in clinopyroxene (Taylor and Neal 1989). The former had been interpreted as high-pressure cumulates and the latter as relics of a subducted oceanic crust. Selected mineral composition and structural formulae from the samples analyzed in this paper are reported in the electronic supplementary material.

Major elements

Eclogite xenoliths from both Roberts Victor and Jagersfontein are eclogites sensu stricto, with Na/(Na + Ca) in clinopyroxene > 0.20 (Clark and Papike 1968), and have a wide range in omphacite K_2O contents (~ 0.02–0.34 wt%) and garnet Na_2O contents (~ 0.01–0.16 wt%). They are roughly equally distributed among the Types IA, IB and IIA, IIB (as previously defined by Huang et al. 2012), respectively (Fig. 4), with variable FeO (6.23–21.62 wt%) and MgO (4.59–20.63 wt%) garnet content. There are three main compositional clusters for garnet endmembers: $Py_{35–40}Alm_{20–40}Grs_{20–35}$; $Py_{40–45}Alm_{15–30}Grs_{20–40}$ and $Py_{45–75}Alm_{20–45}Grs_{5–15}$ and the samples range from groups A to C after Taylor and Neal (1989) (Fig. 5a) also shown by the wide spread in clinopyroxene composition with negatively correlated Na_2O (1.11–8.81 wt%) and MgO (4.82–17.54 wt%) composition. Similarly, the omphacite compositions cover a broad range in Al_2O_3 and Na_2O (~ 7–64% jadeite component), with a positive correlation (Fig. 5b).

Kyanite-bearing samples from this study also cover a wide compositional range and belong to both the metasomatized—Type I and pristine—Type II categories (Radu et al. 2017), as well as in the transitional group. Garnet is typically MgO poor (~ 4.6–11.4 wt%). All metasomatized

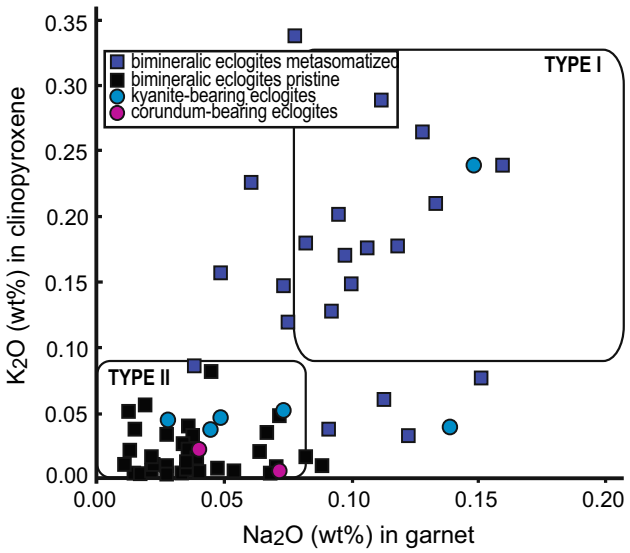

Fig. 4 Na_2O in garnet vs. K_2O in clinopyroxene for eclogite xenoliths from Roberts Victor and Jagersfontein mines. Bimineralic eclogites showing metasomatic textural traits (i.e., indented grain boundaries, numerous melt inclusions and secondary minerals) are marked with dark blue solid square symbols and eclogites with pristine textures are marked with black solid square symbols. Si–Al-rich eclogites are marked with blue (ky-bearing) and violet (cor-bearing) solid circle symbols. The two Type I and Type II fields are delimited as defined by McCandless and Gurney (1989) and Huang et al. (2012)

kyanite eclogites are characterized by low garnet FeO (~ 10.8–14.4 wt%) and jadeite-rich clinopyroxene ($Jd_{50–57}$) and are classified as Type IB and IK (after Huang et al. 2012). Our non-metasomatized samples belong to the Type IIB group, except for RV333, which is a Type IIA. All kyanite-bearing eclogites are classified as Group B and Group C (Fig. 5) after Taylor and Neal (1989) and, with the exception of the two pyrope-rich samples, they

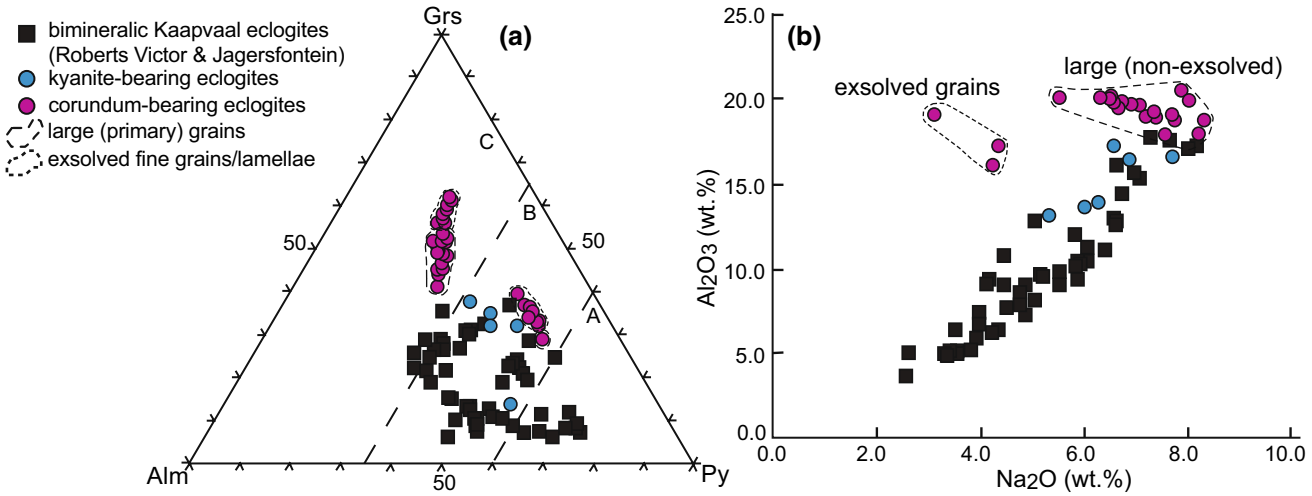

Fig. 5 Ternary grossular (Grs)–pyrope (Py)–almandine (Alm) plot (molar proportions) in garnet (**a**) and Na_2O vs. Al_2O_3 plot in clinopyroxene (**b**) in eclogite xenoliths from the Kaapvaal craton comprising samples from Roberts Victor and Jagersfontein mines. Bimineralic eclogites are marked with black square solid symbols, ky-eclogites with blue solid circle symbols and cor-eclogites with purple solid circle symbols. A, B, C groups are delimited as defined by Taylor and Neal (1989)

are typically characterized by grossular-rich garnet and jadeite-rich clinopyroxene.

Corundum is restricted to the Type II—pristine eclogites (Fig. 4) that have very low clinopyroxene K_2O content (0.01–0.02 wt%). The large, primary, garnet grains have higher MgO (14.9–16.5 wt%), specific to Type IIA, with respect to garnet exsolutions (4.59–11.8 wt% MgO), classified as Type IIB. Clinopyroxenes with exsolution textures are typically more magnesian (~ 5.97–9.98) and less sodic and aluminous (~ 4.07–5.51 wt% Na_2O; 14.0–19.9 wt% Al_2O_3), with lower Ca-Tschermack (Ca-Ts) (~ 0.11–0.37) than non-exsolved, primary grains (~ 4.82–9.07 wt% MgO; 3.07–7.87 wt% Na_2O; 16.5–20.4 wt% Al_2O_3; 0.16–0.51 CaTs). The Na and Mg content in clinopyroxene and the typically grossular-rich garnets with distinct trends towards Ca-enrichment for the exsolutions (Fig. 5), place corundum eclogites in groups B and C after Taylor and Neal (1989), proportional to their degree of exsolution.

Temperatures have been calculated with the garnet-clinopyroxene Fe–Mg geothermometer proposed by Krogh (1988) for 1 GPa, 3 GPa and 6 GPa, and the tendency lines were intercepted with the local conductive model geotherm (Pollack and Chapman 1977) that corresponds to a 39 mW m^{-2} surface heat flow (Griffin et al. 2003). Metasomatized, Type I eclogites, cover a wide range in pressure–temperature conditions, of ~ 800–1300 °C and ~ 3.2–6.5 GPa. Nevertheless, these temperatures remain unreliable, due to possible chemical disequilibrium induced by the percolating fluids. The non-metasomatized, bimineralic eclogites show a bi-modal distribution, where Type IIA corresponds to lower PT conditions (~ 650–1000 °C; ~ 2.0–4.5 GPa) than Type IIB (~ 1000–1300 °C; ~ 4.5–6.5 GPa). This indicates a compositionally stratified distribution of eclogites in the SCLM. PT equilibrium conditions yielded by ky- and cor- bearing eclogites are overall higher (~ 960–1150 °C; 4.1–5.6 GPa and ~ 950–1300 °C; 4.0–6.5 GPa, respectively) than the PT estimates for bimineralic eclogites specific for the lowermost part of the cratonic keel.

Trace elements

The previously defined Type I eclogites from this study are characterized by a narrow LREE and LILE concentration range, with variable degrees of LREE/HREE fractionation. Clinopyroxene has convex upward REE patterns, with $(La/Nd)_N$ of 0.16–0.56 and $(Nd/Yb)_N$ of 5.33–76.2 (subscript *N* denominates values normalized to the primitive mantle McDonough and Sun 1995). The Sr clinopyroxene concentration ranges between 2.5 and 19.9, roughly overlapping the ~ 5.0–15.1 estimated values for eclogitic clinopyroxene (Jacob et al. 2003). Garnet REE spectra have strongly fractionated LREE ($(La/Nd)_N$ of 0.005–0.26) and generally flat MREE-HREE ($(Nd/Yb)_N$ of 0.03–0.89). We distinguish two compositional groups, characterized by HREE-rich garnet (between 8 and 11 times the primitive mantle) and HREE-poor garnet (between 1.5 and 3 times).

Our Type II eclogites comprise two compositional groups and associated LREE and LILE distribution patterns, for both garnet and clinopyroxene (Fig. 6a, b). The first group predominantly consists of Type IIA eclogites and is characterized by clinopyroxene with LREE concentrations superior to the primitive mantle values (between 1 and 30 times primitive mantle). The clinopyroxene REE patterns have flat LREE distribution ($(La/Nd)_N$ of 0.20–1.38) and

strongly fractionated MREE-HREE $(Nd/Yb)_N$ of 3.43–167.1 (Fig. 6a). The primitive mantle-normalized clinopyroxene Sr concentration ranges between 1.42 and 39.0. All extended trace element spectra of clinopyroxene are strongly fractionated $(Nb/La)_N$ ratio (0.001–0.50), and show positive Sr anomalies (1.71–30.0 Sr*, $Sr^* = Sr_N/sqrt(Sm_N*Nd_N)$) (Fig. 6c). Similarly, garnet has high and slightly fractionated LREE profiles $((La/Nd)_N$ of 0.01–0.05), and flat MREE-HREE distribution $((Nd/Yb)_N$ of 0.08–1.68). The extended trace elements spectra have $(Nb/La)_N$ of 0.68–25.6 and weak positive Zr inflections are observed in garnet (Fig. 6b, d).

The second compositional group includes both Type IIA and IIB eclogites (Fig. 6) and is defined by sub-primitive mantle LREE concentrations in clinopyroxene (nine times lower than primitive mantle values). REE patterns typically have fractionated LREE $((La/Sm)_N$ of 0.03–0.01), less pronounced for HREE $((Sm/Yb)_N$ of 4.04–13.2). Sr content in clinopyroxene (0.51–1.22 Sr_N) is inferior to the LREE-rich group and typical eclogitic values. Although less pronounced, all LREE-poor clinopyroxene have positive Sr anomalies (Sr* 1.40–7.95). Garnet composition is LREE depleted, with strongly fractioned $(La/Sm)_N$ of 0.001–0.03 and flat or slightly enriched HREE distribution $((Sm/Yb)_N$ of 0.20–2.83). The extended trace element patterns show negative inflections in Zr and Hf.

Kyanite-bearing eclogites have convex upward clinopyroxene REE patterns (Fig. 7), with fractioned LREE (0.03–9.39 $(La/Nd)_N$) and HREE (19.6–114 $(Nd/Lu)_N$).

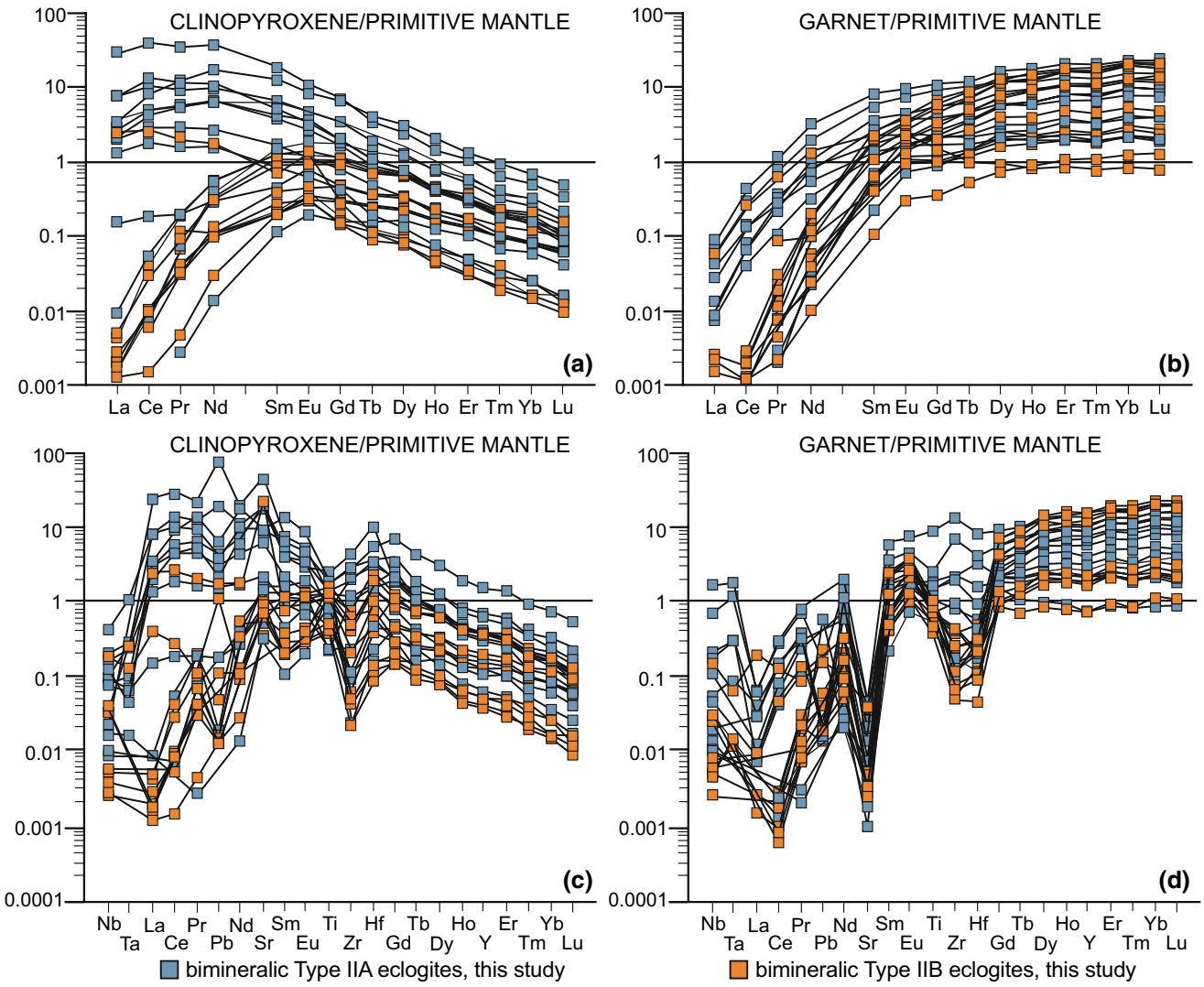

Fig. 6 REE (**a, b**) and extended trace elements patterns (**c, d**) in clinopyroxene and garnet, normalized to the primitive mantle (McDonough and Sun 1995), in bimineralic, Type II (non-metasomatized) eclogites from the Kaapvaal craton comprising samples from Roberts Victor and Jagersfontein mines. Type IIA (Mg rich) are marked with blue solid square symbols and Type IIB (Mg poor) with orange solid square symbols

Sr primitive mantle-normalized concentrations are typically between ~5 and 22 times higher than primitive mantle values. Garnet REE spectra have fractionated LREE (0.003–0.06 $(La/Sm)_N$) and flat HREE with 1.08–1.97 $(Sm/Yb)_N$. All samples have positive Sr anomalies in clinopyroxene (4.78–26.1 Sr*). Similarly, both clinopyroxene and garnet have positive Eu anomalies (Eu^*_{cpx} 1.05–1.55, Eu_{gt} 1.06–3.97, $Eu^* = Eu_N/sqrt(Sm_N*Gd_N)$), except for sample RV168 where they are preserved only in the garnet fraction. The extended incompatible element patterns show additional positive inflections for Pb and Hf in clinopyroxene and equivalent negative inflections in garnet.

Minerals in corundum-bearing eclogites have overall incompatible elements concentrations lower than the primitive mantle (Fig. 7). Sample RV179 has fractionated LREE and MREE ($(La/Sm)_N = 2.97$) and HREE-enriched ($(Sm/Lu)_N = 0.79$) clinopyroxene patterns; and convex downward garnet REE spectra, with fractionated LREE and MREE ($(La/Sm)_N = 0.16$) and flat HREE ($(Sm/Lu)_N = 0.44$). Sample RV344 has convex upward clinopyroxene patterns ($(La/Sm)_N = 0.03$; $(Sm/Lu)_N = 10.4$) and garnet REE patterns with strongly fractionated LREE ($(La/Sm)_N = 0.003$) and MREE ($(Sm/Dy)_N = 0.47$) and flat HREE ($(Sm/Lu)_N = 1.02$), higher than the primitive mantle. Both samples have positive Eu anomalies in clinopyroxene and garnet (Eu^*_{cpx} 1.11–4.91, Eu^*_{gt} 1.13–4.16), and sample RV179 shows positive Sr anomaly in clinopyroxene (Sr* = 12.7).

Oxygen isotopes

The $\delta^{18}O$ values of garnet, clinopyroxene, kyanite and corundum from this study (Table 1) range from higher to significantly lower than the mantle ($+5.5 \pm 0.4‰$ Mattey

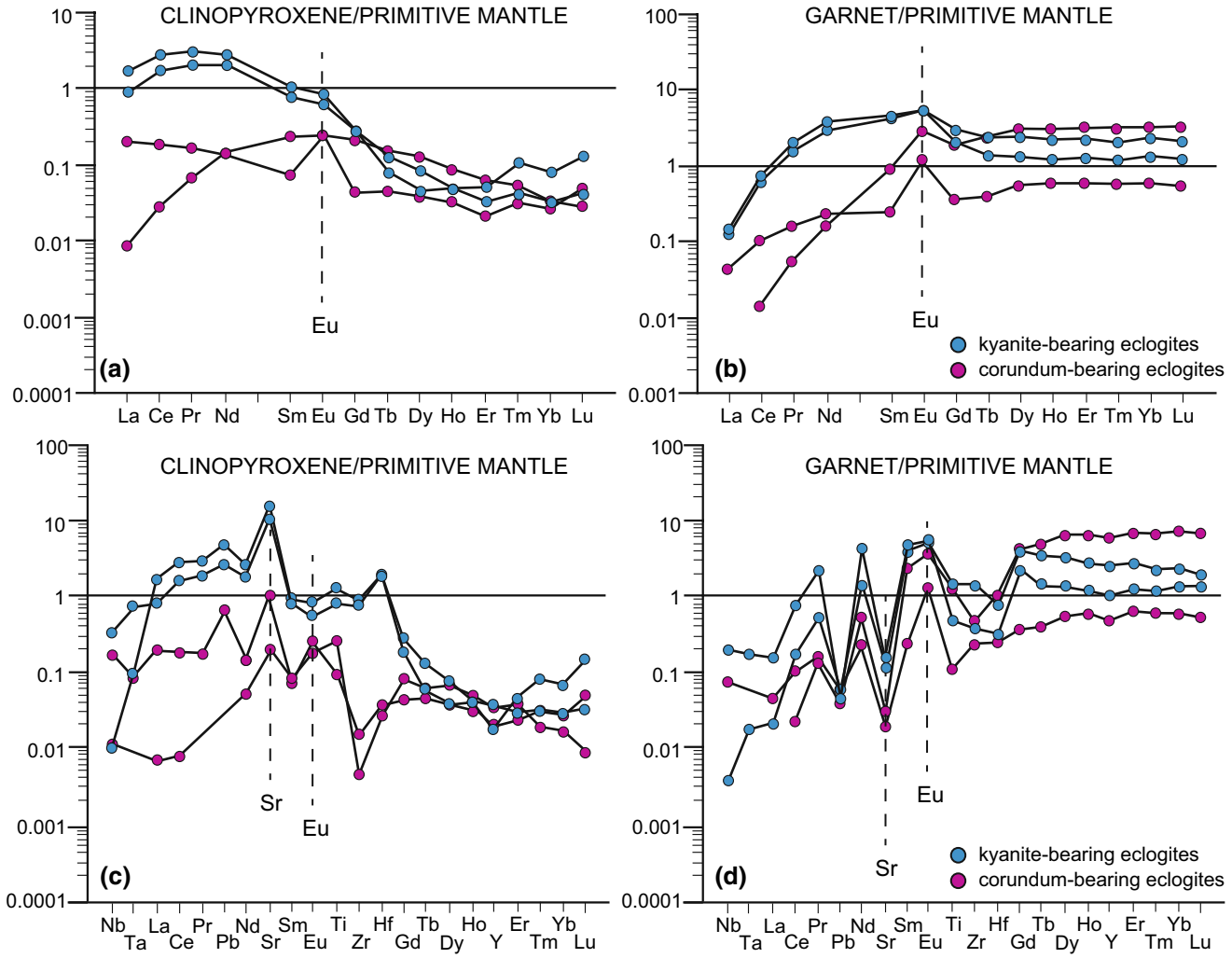

Fig. 7 REE (**a, b**) and extended trace elements patterns (**c, d**) in clinopyroxene and garnet, normalized to the primitive mantle (McDonough and Sun 1995), in kyanite (blue solid circle symbols) and corundum eclogites (violet solid circle symbols) from Roberts Victor and Jagersfontein mines

et al. 1994) (Fig. 8). Whole-rock $\delta^{18}O$ values estimated from mineral $\delta^{18}O$ values and modal proportions (see "Analytical techniques" for method) vary from 1.4‰ to 7.5‰.

Three metasomatized (Type I) samples have been analyzed for comparison. The $\delta^{18}O$ values of garnet range from 5.4 to 6.1‰. Among the non-metasomatized eclogites, we distinguish low-$\delta^{18}O$ eclogites, which have garnet values ranging from 1.1 to 4.8‰ in agreement with the coexisting clinopyroxene (1.4–4.9‰), and high-$\delta^{18}O$ eclogites, with mineral $\delta^{18}O$ values that range from the expected ranges for peridotitic mantle (5.2–6.0‰ in garnet and 5.2–6.0‰ in clinopyroxene), to higher values (6.0–7.5‰ in garnet and 5.5–7.5‰ in clinopyroxene).

The low-$\delta^{18}O$ group includes bimineralic samples, as well as corundum-bearing eclogites. The former have garnet values between 2.3 and 3.9‰ and between 4.5 and 4.8‰ (Fig. 9). The lowermost values typically correspond to the low-magnesium (Type IIB) eclogites characterized by high-pressure–temperature equilibrium conditions, whereas the higher $\delta^{18}O$ values correspond exclusively to the magnesium-rich, Type IIA eclogites, characterized by lower PT conditions. Similarly, the high-$\delta^{18}O$ group with mantle-like or higher $\delta^{18}O$ values corresponds strictly to Type IIA eclogites (Fig. 9). The corundum-bearing eclogites have $\delta^{18}O$ values lower than the 'normal' mantle, with whole rock estimates of 1.4 and 4.8‰. Moreover, sample RV344 has the lowest $\delta^{18}O$ values recorded so far in mantle eclogites, with a garnet average of 1.1 ($n=4$, $1\sigma=0.22$). By contrast, kyanite-bearing (~5.6–6.7‰) eclogites have greater than equal to 'normal' mantle $\delta^{18}O$ values.

Discussion

Origin and evolution of mantle eclogites

Extensively metasomatized eclogites can be distinguished from non-metasomatized eclogites based on their destabilized textures (e.g., serrated grain boundaries, abundant melt inclusions), high alkali and LREE compositions (Aulbach et al. 2016; Aulbach and Viljoen 2015; Gréau et al. 2011; Huang et al. 2012). Although some authors have attempted to recalculate the composition of pristine eclogites from metasomatized samples, (Aulbach and Jacob 2016; Aulbach and Viljoen 2015), it is the non-metasomatized eclogites that most likely represent the closest composition to their protolith (Gréau et al. 2011; Radu et al. 2017).

The Archaean Earth would have had higher mantle heat-flow expressed as potential temperature T_P (McKenzie and Bickle 1988), leading to a higher degree of adiabatic melting compared to modern mid-oceanic ridge (MOR) settings (Herzberg 2011). In this situation, the primary magmas would have had higher Mg and lower Si and Na contents compared to present-day MOR basalts or boninites (Aulbach and Jacob 2016; Herzberg and O'Hara 1998; Jacob and Foley 1999). The average potential protolith made of Archaean oceanic crust is, therefore, assumed to be compositionally equivalent to picrite (MgO ~ 22.0 wt%) (Aulbach and Viljoen 2015; Jacob and Foley 1999; Schmickler et al. 2004). For comparison, a basaltic composition corresponding to modern MOR is assumed, as well as gabbro for low-pressure plagioclase-rich cumulate, with granophyre as the most evolved term of an evolving mafic magma (Fig. 11).

Bimineralic eclogites

Metasomatized eclogites

The Type I (Na_2O in garnet > 0.9 wt%; K_2O in omphacite > 0.8 wt%), metasomatized eclogite, from our study has textural aspects consistent with fluid interaction: numerous inclusions, indented crystal boundaries and subrounded to rounded grains. The reconstructed whole rock trace elements composition of metasomatized eclogites duplicates the two previously observed compositional groups characterized by HREE-rich (8–11 times the primitive mantle) and HREE-poor (1.5–3 times the primitive mantle) garnets (Fig. 10). The former shows typically flat REE profiles with slightly fractionated LREE, $(La/Sm)_N$ of 0.10–0.56 and $(Sm/Lu)_N$ of 0.31–0.83, similar to a tholeiitic basalt composition (Fig. 10a, c). The latter group shows comparable LREE distribution, $(La/Sm)_N$ of 0.05–0.55 and more fractionated HREE, $(Sm/Lu)_N$ of 1.53–3.73, with significantly lower MREE-HREE concentrations (Fig. 10b, d). There is a distinct correlation between the amount of HREE (Sm–Lu) and the FeO and CaO contents in garnet. Eclogites containing garnets with low-Ca and high-Fe contents typically have high-bulk ΣHREE, whereas samples with Ca-rich, Fe-poor garnets have low-bulk ΣHREE composition. This could be due to the substitution of HREE for Ca, more markedly in the garnet than in the clinopyroxene structure, controlled by similar ionic radii (Harte and Kirkley 1997) or to enrichment by silicate melts (Aulbach et al. 2016).

Non-metasomatized eclogites

The Type II eclogite xenoliths from this study are in apparent textural equilibrium, with translucent subhedral grains, showing no evidence of extensive metasomatism and are characterized by garnet with $Na_2O < 0.9$ wt% and K_2O in omphacite < 0.8 wt%. The reconstructed whole-rock compositions of non-metasomatized eclogites correlate with the previously described compositional types IIA and IIB.

Type IIA eclogite bulk compositions are rich in MgO (11.15–19.71 wt%) and vary broadly from low to high CaO (5.85–17.52 wt%), Al_2O_3 (6.23–22.18 wt%) and Na_2O

Table 1 $\delta^{18}O$ values (the ‰ deviation from $^{18}O/^{16}O$ in the standard) of garnet, clinopyroxene, kyanite, corundum and recalculated bulk rock based on mineral abundance in eclogite xenoliths from Roberts Victor and Jagersfontein mines, South Africa. PT estimates were determined with Krogh (1988) geothermometer, see "Major elements" for method

Sample	Type	Garnet	Cpx	Kyanite	Corundum	Bulk $\delta^{18}O$	T (°C)	P (GPa)	Locality
JG29	II A	6.52	5.78	–	–	6.15	950	4.1	Jagersfontein
JG29r	II A	6.18	5.54	–	–	5.86			Jagersfontein
JG32	II B	3.55	3.73	–	–	3.64	1115	5.3	Jagersfontein
JG32r	II B	3.14	3.49	–	–	3.31			Jagersfontein
JG33	II A	7.73	7.47	–	–	7.49	943	4.1	Jagersfontein
JG33r	II A	–	7.28	–	–	–			Jagersfontein
JG33r	II A	7.50	7.54	–	–	7.54			Jagersfontein
RV159	II A	6.60	6.59	–	–	6.59	907	3.8	Roberts Victor
RV168	ky-bearing	6.27	6.41	6.58	–	6.45	1087	5.0	Roberts Victor
RV174	II A	4.67	4.60	–	–	4.64	955	4.1	Roberts Victor
RV177	II A	3.29	3.30	–	–	3.29	893	3.7	Roberts Victor
RV179	cor-bearing	4.72	4.89	–	4.77	4.84	nd	nd	Roberts Victor
RV179r	cor-bearing	5.34	5.11	–	–	–			Roberts Victor
RV180	II A	3.10	2.89	–	–	3.00	854	3.5	Roberts Victor
RV186	II B	2.99	3.12	–	–	3.05	1211	6.1	Roberts Victor
RV197	II A	4.67	4.56	–	–	4.61	800	3.1	Roberts Victor
RV199	II B	3.37	3.33	–	–	3.35	1341	7.3	Roberts Victor
RV203	II A	3.73	3.28	–	–	3.50	780	3.1	Roberts Victor
RV203r	II A	3.05	–	–	–	–			Roberts Victor
RV209	ky-bearing	5.32	5.76	5.69	–	5.62	979	4.3	Roberts Victor
RV218	ky-bearing	6.48	6.78	–	–	6.71	1229	6.3	Roberts Victor
RV220	II B	2.59	2.17	–	–	2.38	1089	5.1	Roberts Victor
RV220r	II B	2.12	2.54	–	–	2.33			Roberts Victor
RV221	II B	3.69	4.09	–	–	3.89	1117	5.3	Roberts Victor
RV221r	II B	3.55	3.75	–	–	3.65			Roberts Victor
RV226	I A	6.12	6.08	–	–	6.10	1026	4.6	Roberts Victor
RV233	II B	3.61	3.69	–	–	3.65	1176	5.8	Roberts Victor
RV233r	II B	3.59	3.61	–	–	3.60			Roberts Victor
RV234	II B	3.48	3.47	–	–	3.47	1150	5.6	Roberts Victor
RV319	ky-bearing	5.65	5.71	5.95	–	5.75	1144	5.5	Roberts Victor
RV320	ky-bearing	5.54	5.99	5.89	–	5.76	1147	5.6	Roberts Victor
RV344	cor-bearing	0.98	0.86	–	–	–	1097	5.2	Roberts Victor
RV344r	cor-bearing	1.43	1.36	–	1.17	1.37			Roberts Victor
RV344r	cor-bearing	0.94	–	–	–	–			Roberts Victor
RV344r	cor-bearing	1.08	–	–	–	–			Roberts Victor
RV347	II A	4.82	4.90	–	–	4.86	926	3.9	Roberts Victor
RV355	II A	3.84	3.63	–	–	3.71	755	2.9	Roberts Victor
RV355r	II A	3.99	3.63	–	–	3.78			Roberts Victor
RV360	II A	5.25	5.18	–	–	5.24	804	3.1	Roberts Victor
RV377	II A	3.88	3.80	–	–	3.83	nd	nd	Roberts Victor
RV377r	II A	3.84	3.63	–	–	3.71			Roberts Victor
RV469	II B	–	2.40	–	–	–	1251	6.4	Roberts Victor
RV469r	II B	2.35	2.40	–	–	2.38			Roberts Victor
RV488	II A	5.47	5.19	–	–	5.39	674	2.5	Roberts Victor
RV488r	II A	–	5.29	–	–	–			Roberts Victor
RV508	II A	4.37	–	–	–	–	868	3.6	Roberts Victor
RV508r	II A	4.56	4.59	–	–	4.58			Roberts Victor
RV508r	II A	4.43	–	–	–	–			Roberts Victor
RV513	II A	5.23	5.58	–	–	5.40	1249	6.3	Roberts Victor

Δcpx-gt is the permil difference calculated as $\delta^{18}O_{cpx}–\delta^{18}O_{gt}$. Replicate measurements are marked with "r" and "nd" denotes samples for which the PT estimates could not be obtained

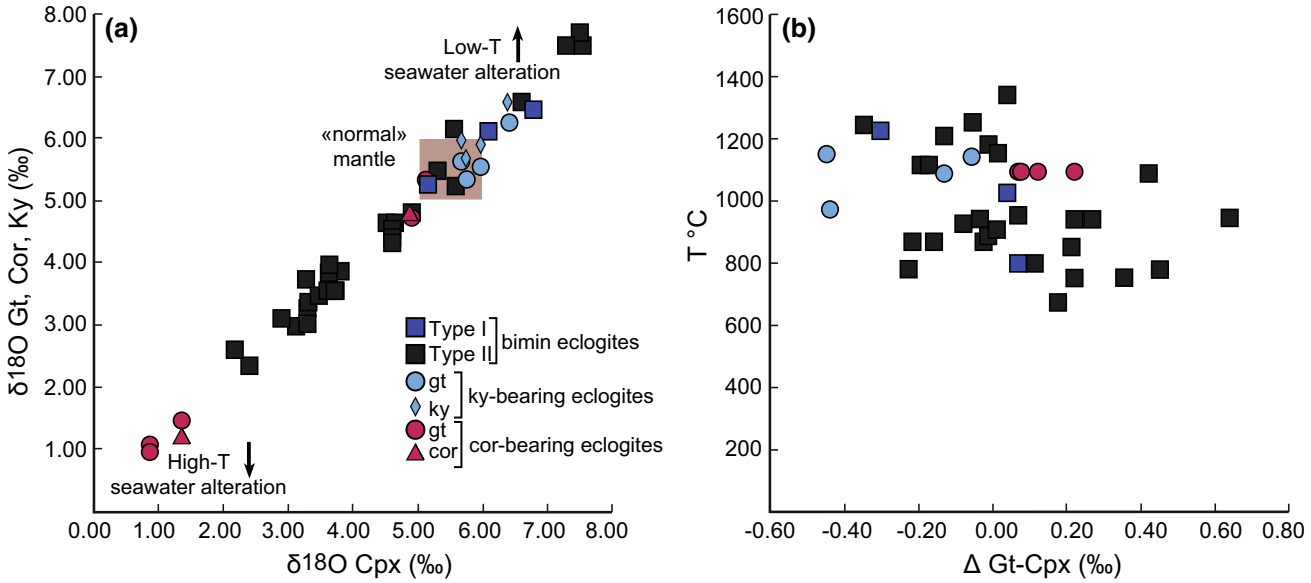

Fig. 8 Plot of **a** $\delta^{18}O$ values of garnet (gt), corundum (cor) and kyanite (ky) vs. clinopyroxene (cpx) from this study; **b** Δ_{gt-cpx} vs. temperature (°C) calculated from Fe–Mg exchange between garnet and clinopyroxene after Krogh (1988). Metasomatized (Type I) bimineralic eclogites (Roberts Victor mine) are marked with dark blue solid square symbol. Non-metasomatized (Type II) bimineralic eclogites are marked with black solid square symbols. Ky-cor-bearing samples are marked with light blue (kyanite) and violet (corundum) solid circle (gt), diamond (ky) and triangle (cor) symbols. Red solid square marks 'normal' mantle values 5.5 ± 0.4‰ (Mattey et al. 1994). Analytical error bars are inferior to the symbol size

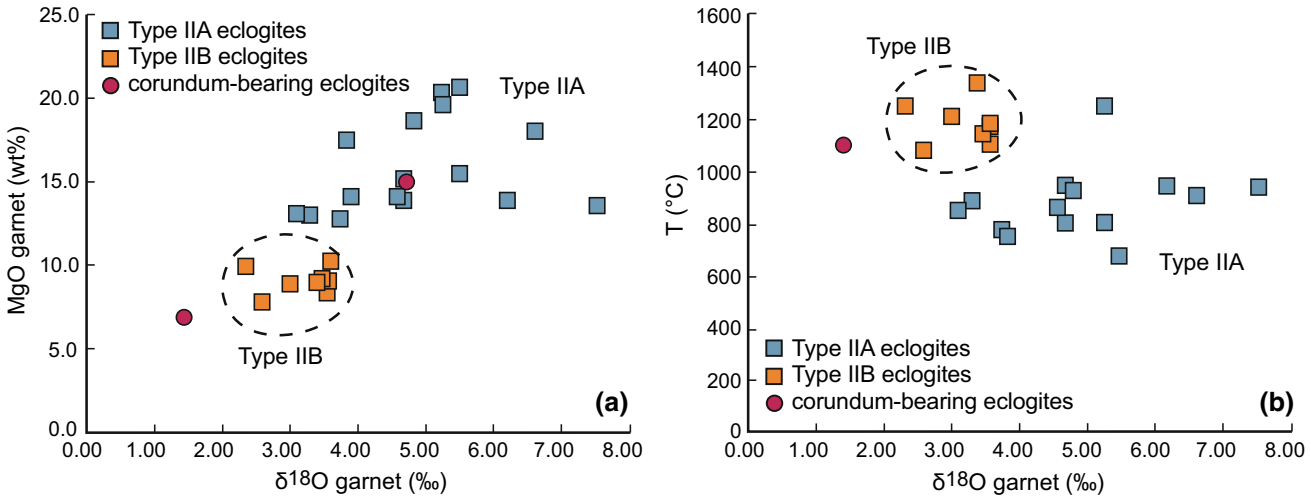

Fig. 9 Garnet $\delta^{18}O$ vs. **a** MgO in garnet and **b** temperature (°C) calculated from Fe–Mg exchange between garnet and clinopyroxene after Krogh (1988) in bimineralic Type II (non-metasomatized) and corundum-bearing eclogites from this study. Pristine eclogites with Mg-rich garnets (Type IIA) have generally higher $\delta^{18}O$ values and correspond to lower PT conditions. Non-metasomatized eclogites with Mg-poor garnets (Type IIB) have lower $\delta^{18}O$ values and correspond to higher PT equilibrium conditions. Type IIA is marked with blue solid square symbols, Type IIB with orange solid square symbols and corundum-bearing eclogites are marked with violet solid circle symbols

(0.17–4.27 wt%) contents (Fig. 11). The decreasing Mg# could be following olivine (± pyroxene) fractionation in an oceanic crustal protolith, translated also by the increasing FeO content (Aulbach and Viljoen 2015). Furthermore, Type IIA eclogites systematically show an inverse correlation between Na_2O and Al_2O_3 content with respect to MgO (Fig. 11c, d), which can be equally accounted for by progressive fractional crystallization of olivine ± pyroxene in an evolving "basaltic" liquid (Aulbach et al. 2016). The high CaO and, less marked, Al_2O_3 contents at relatively constant

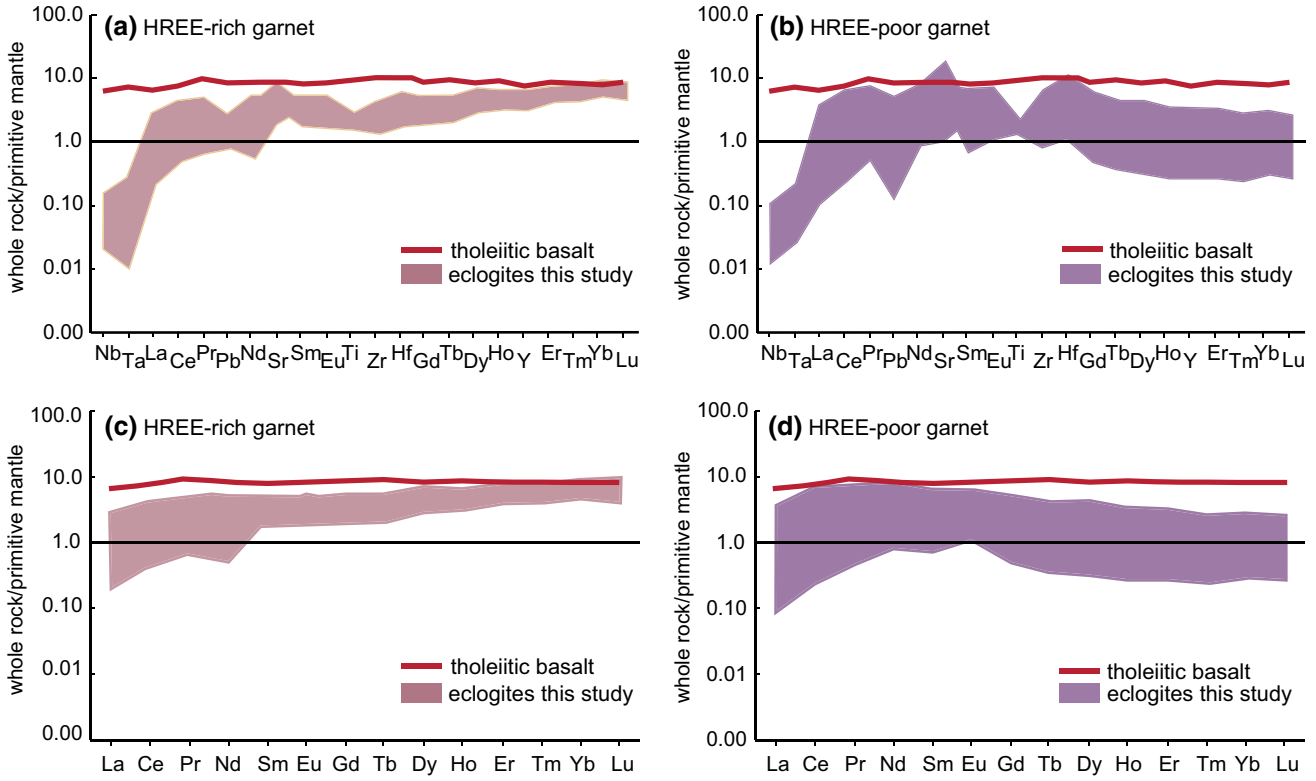

Fig. 10 Reconstructed whole-rock extended trace (**a, b**) and REE patterns (**c, d**) in bimineralic Type I (metasomatized) eclogites from the Kaapvaal craton compared to tholeiitic basalt composition (GEOROC compilation). Primitive mantle values are from McDonough and Sun (1995)

MgO are interpreted as evidence for a small fraction of plagioclase (±diopsidic clinopyroxene) accumulation, as main mineral phases preferentially incorporating Ca with respect to Mg (Beard et al. 1996). The REE and extended incompatible trace element patterns of reconstructed Type IIA whole-rock compositions (Fig. 12a, b) are predominantly flat and superior to primitive mantle values (0.8–20 times higher). These compositions are comparable to average oceanic picrite content with the exception of Nb, Ta and La. Moreover, Type IIA eclogites show positive correlation between ΣREE and Y concentrations, with respect to TiO_2 content. It is inferred that REE and HFSE enrichment is caused by olivine fractionation (Aulbach et al. 2016). All Type IIA eclogites register positive Eu* (1.06–2.71) and Sr* (1.11–12.21) anomalies, inversely correlated with TiO_2 content (Fig. 11e, f). This is in agreement with the previous inference, arguing for the presence of plagioclase in a protolith issued from an evolved picritic liquid for Type IIA eclogites (Beard et al. 1996; Jacob and Foley 1999).

The reconstructed bulk rock compositions of Type IIB eclogites have low MgO (6.93–10.12 wt%) and medium to high CaO (10.66–15.54 wt%), Al_2O_3 (14.26–20.10 wt%) and Na_2O (2.58–3.96 wt%) contents. Covering a lower and narrower range of values, MgO content shows a similar positive correlation with Mg# and inverse correlation with Al_2O_3 and Na_2O as for Type IIA eclogites (Fig. 11a–d). It is inferred the progressive enrichment in Al_2O_3 and Na_2O along with MgO depletion is the result of olivine (±pyroxene) fractional crystallization in oceanic crust (Aulbach et al. 2016; Aulbach and Viljoen 2015), precursory to the eclogite formation. Concurrently, iron oxide crystallization and plagioclase accumulation could lead to progressive FeO decrease and CaO increase, respectively. The REE and extended incompatible elements patterns of reconstructed Type IIB whole-rock compositions (Fig. 12c, d) have strongly fractionated LREE ($(La/Sm)_N$ ~ 0.001) and flat to slightly enriched MREE-HREE ($(Sm/Lu)_N$ ~ 0.07–0.19) predominantly higher than primitive mantle values (~5–10 times). The high-HREE concentrations, with flat to enriched distribution, are similar to average picrite or tholeiitic basalt compositions. Strongly fractionated LREE may be the result of partial melt loss during burial. All samples have negative Zr and Hf anomalies, which could indicate a metasomatic HFSE depletion of the protolith source (Aulbach et al. 2011). Most Type IIB samples have positive Eu* (0.90–1.61), with variable Sr* (0.18–3.78) from negative to positive anomalies, inversely correlated with TiO_2 content and have a positive correlation between ΣREE and Y concentrations with respect to

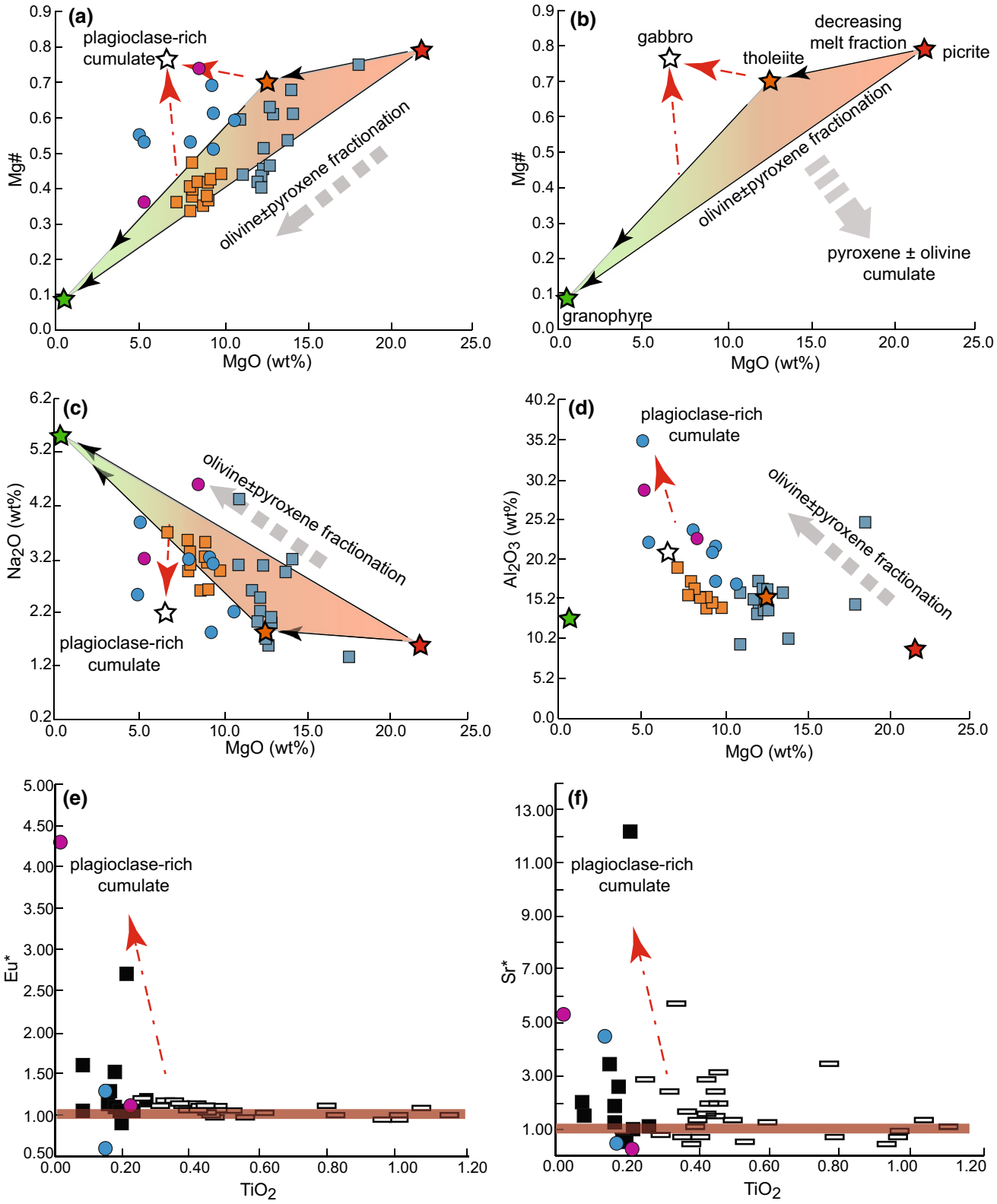
(a)
plagioclase-rich cumulate
olivine±pyroxene fractionation
Mg#
MgO (wt%)
(b)
gabbro
tholeiite
decreasing melt fraction
picrite
olivine±pyroxene fractionation
pyroxene ± olivine cumulate
granophyre
Mg#
MgO (wt%)
(c)
olivine±pyroxene fractionation
plagioclase-rich cumulate
Na2O (wt%)
MgO (wt%)
(d)
plagioclase-rich cumulate
olivine±pyroxene fractionation
Al2O3 (wt%)
MgO (wt%)
(e)
plagioclase-rich cumulate
Eu*
TiO2
(f)
plagioclase-rich cumulate
Sr*
TiO2
Type IIA bimineralic eclogite;
kyanite-bearing eclogite;
corundum-bearing eclogite;
Type IIB bimineralic eclogite;
granophyre;
picrite;
Type II bimineralic eclogite;
gabbro
olivine-bearing tholeiite;

◂**Fig. 11** Relationships between major elements, Eu* (Eu* = Eu_N/sqrt(Sm_N*Gd_N)) and Sr* (Sr* = Sr_N/sqrt(Sm_N*Nd_N)) in reconstructed whole-rock compositions of bimineralic Type II (non-metasomatized) eclogites, kyanite- and corundum-bearing eclogites from the Kaapvaal craton, and magma series endmembers (from GEOROC compilation). The ultramafic pole is represented by Icelandic picrite and the mafic pole by olivine-bearing tholeiite, whereas the felsic endmember is represented by granophyre and a plagioclase cumulate composition is represented by gabbro. The subscript "*N*" shows primitive mantle-normalized concentrations (McDonough and Sun 1995)

TiO_2 content, interpreted as the result of olivine fractionation (Aulbach and Viljoen 2015). These composition trends support the interpretation that Type IIB eclogites are derived from a picritic to basaltic protolith which underwent differentiation, (Aulbach et al. 2016; Beard et al. 1996; Jacob 2004; Jacob and Foley 1999; Taylor and Neal 1989), followed by small degrees of partial melting during eclogitization and burial (Schulze et al. 2000; Shervais et al. 1988; Viljoen et al. 2005).

High-Al eclogites

The kyanite- and corundum-bearing eclogites have low reconstructed bulk MgO content (5.37–11.47 wt%), and have medium to high CaO (13.03–17.54 wt%) and Al_2O_3 (22.62–33.34 wt%) contents. The FeO content (1.84–7.43 wt%) progressively decreases from kyanite- to corundum-bearing eclogites. Conversely, Na_2O (1.78–4.56 wt%) and Mg# progressively increase from kyanite-(0.34–0.69) to corundum-bearing eclogites (0.71–0.75) (Fig. 11a-d) without a strong variation of MgO content, interpreted as evidence for a protolith dominated by plagioclase accumulation possibly concurrent with iron oxide crystallization (Agashev et al. 2018; Schulze et al. 2000; Shervais et al. 1988; Shu et al. 2016).

Reconstructed bulk trace element compositions of kyanite-bearing eclogites (Fig. 13a, b) have REE patterns with poorly fractionated, enriched LREE ($(La/Sm)_N$ 0.61–1.18) and slightly fractionated to flat HREE ($(Sm/Lu)_N$ 2.83–3.94). These incompatible element concentrations are similar to a gabbroic composition and are marked by positive Eu* (1.31–1.46) and Sr* (1.63–4.61) anomalies (Jacob 2004). This is further supported by decreasing TiO_2 contents with ΣREE and Y, interpreted as evidence for plagioclase accumulation, equally translated into increasing Eu* and Sr*, from negative to positive anomalies, inversely correlated with TiO_2 content (Aulbach et al. 2016). Reconstructed whole-rock composition of corundum-bearing RV179 eclogite (Fig. 13c, d) has flat LREE and HREE, ($(La/Nd)_N$=1.03) and ($(Dy/Lu)_N$=0.88), and concave MREE patterns; incompatible element concentrations inferior to the primitive mantle (~9 times less) and pronounced positive anomalies in Eu and Sr (Eu*=4.32; Sr*=5.38). This is consistent with a pyroxene-plagioclase cumulate protolith. Conversely, corundum-bearing sample RV344 has reconstructed whole-rock trace element compositions with fractionated LREE ($(Ce/Sm)_N$=0.04) and MREE ($(Sm/Dy)_N$=0.39) and almost flat HREE ($(Dy/Lu)_N$=0.88), having MREE-HREE concentrations superior to the primitive mantle (~3 times primitive mantle), and less pronounced Eu-positive anomaly (Eu*=1.12) and negative Sr* anomaly (~0.09). Based on the recalculated bulk rock composition, sample RV344 is interpreted as more likely derived from a gabbroic protolith which has undergone partial melting (Shu et al. 2016).

Pressure–temperature conditions (based on equilibrium Fe–Mg exchange estimated temperatures) for kyanite-bearing eclogites were obtained in the range of ~4.1–5.6 GPa and ~960–1150 °C and at ~4.0–6.5 GPa and ~950–1300 °C for corundum-bearing eclogites. This is coherently sustained by textural and chemical arguments: kyanite-bearing samples exhibit cloudy clinopyroxene, formed through inner structure breakdown by fast decompression, as well as by the high-jadeite and vacancy-bearing CaEsk content in the preserved omphacite cores attesting to their origin from high pressure (Schroeder-Frerkes et al. 2016). Nevertheless, the connection with the bimineralic eclogites and their geometric relation is not yet clear.

Oxygen isotope constraints on eclogite petrogenesis

Oxygen isotopes are robust geochemical tracers because oxygen is ~50% of the rock; and solid-state diffusion rates are slow, even in the mantle (e.g., Peck et al. 2003 and references therein). Crustal material can, therefore, be assumed to preserve its $\delta^{18}O$ values during the process of recycling into the mantle (Jacob et al. 1994; Neal et al. 1990). Moreover, no significant change in $\delta^{18}O$ value would be expected as a result of interaction with potential kimberlite-derived fluids, and mantle metasomatism should change $\delta^{18}O$ values towards a mantle-like range. Numerous studies of eclogites have used oxygen isotopes to constrain their protolith, leading to an important database of $\delta^{18}O$ variations in mantle eclogites. However, many of these studies on South African eclogites are focused on fully (Garlick et al. 1971; Gréau et al. 2011; MacGregor and Manton 1986; Schulze et al. 2000) or partly metasomatized (Riches et al. 2016a) eclogites, and only few non-metasomatized eclogites have been analyzed (Huang et al. 2016; Jacob et al. 2005; Viljoen et al. 2005).

The strong correlation (Fig. 8a) between garnet and omphacite $\delta^{18}O$ values (r^2 = 0.98) is interpreted as evidence that the omphacite $\delta^{18}O$ has not changed with respect to that of the co-existing garnet since their formation. The difference between clinopyroxene and garnet $\delta^{18}O$ values (Δ_{cpx-gt}) ranges from −0.22 to +0.31‰ (n = 35), except for samples:

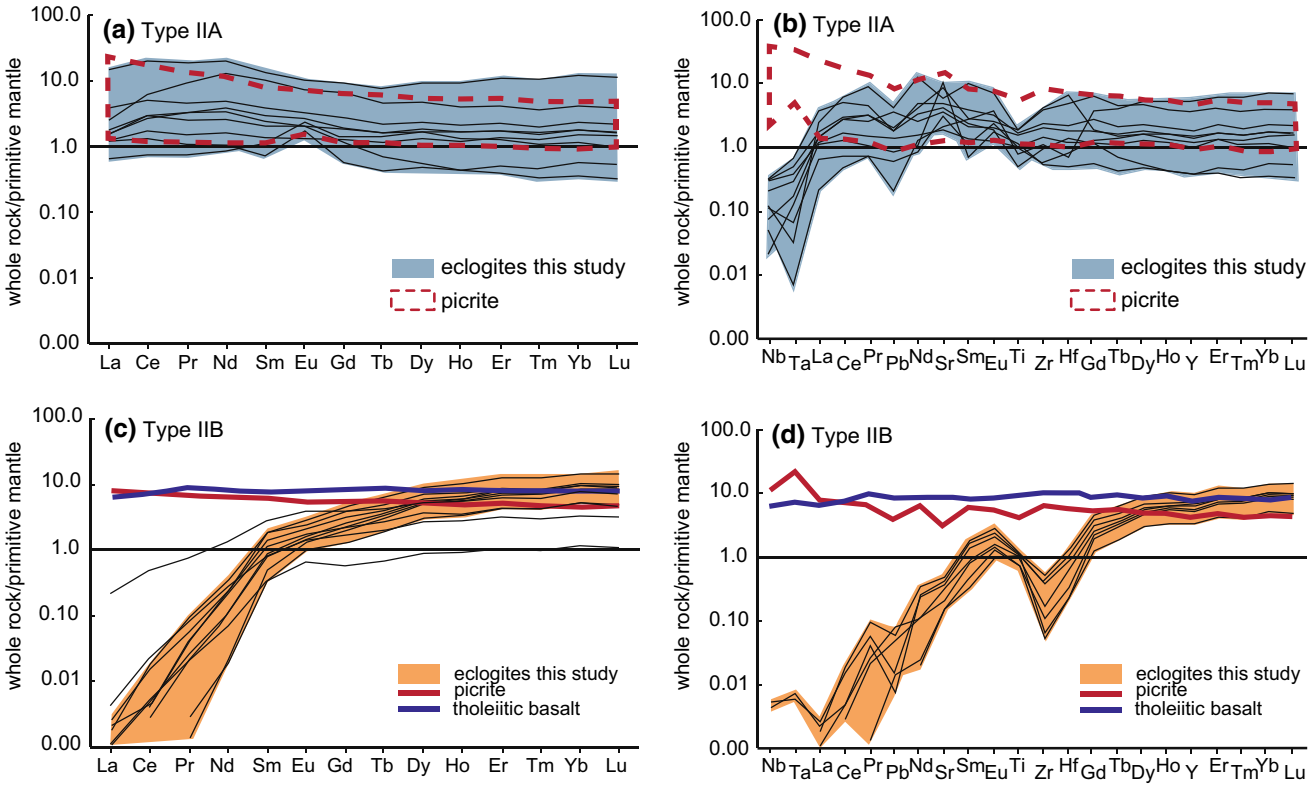

Fig. 12 Reconstructed whole-rock REE (**a, c**) and extended trace elements patterns (**b, d**) in bimineralic Type II (non-metasomatized) eclogites from the Roberts Victor and Jagersfontein mines compared to tholeiitic basalt and picrite compositions (GEOROC compilation). Primitive mantle values are from McDonough and Sun (1995)

JG29 (−0.64 to −0.74‰), RV203 (−0.45‰), RV209 (+0.44‰), RV220 (+0.42‰) and RV320 (+0.45‰); the Δ_{gt-ky} and Δ_{gt-cor} range from −0.37 to −0.30‰ ($n=3$) and from +0.05 and +0.31‰ ($n=4$), respectively. A slight increase in the Δ_{cpx-gt} is observed with increasing temperature (Fig. 8b), contrary to what has been previously observed for Lace eclogites (Aulbach et al. 2017b). Constant differences in $\delta^{18}O$ values in the Δ_{gt-ky} and Δ_{gt-cor} present in each sample is additional evidence for oxygen isotope equilibrium at mantle temperatures. On the basis of the above, it is concluded that the bulk $\delta^{18}O$ values of the eclogite xenoliths estimated from mineral data in this work approximate the $\delta^{18}O$ values of the protolith.

Recalculated bulk rock $\delta^{18}O$ values for the Type IIA (magnesium rich) eclogites vary between 3.0 and 7.5‰. Values lower than average mantle are most easily explained by high-temperature hydrothermal alteration of the original ocean crust, whereas higher than 5.5‰ $\delta^{18}O$ values can be explained by low-temperature alteration (Bindeman 2008). High and low-$\delta^{18}O$ values are present in the upper and lower part of the oceanic crust, respectively (Beard et al. 1996; Eiler 2001; Gregory and Taylor 1981; Jacob et al. 1994; Schulze and Helmstaedt 1988; Shervais et al. 1988). Similarly, we attribute the recalculated bulk rock $\delta^{18}O$ values from 2.3 to 3.9‰, for our Type IIB (low magnesium) eclogites to interaction of oceanic crust with seawater at high temperatures (~350 °C Bowers and Taylor Jr. 1985) (Eiler 2001; Garlick et al. 1971; MacGregor and Manton 1986; Riches et al. 2016a; Shervais et al. 1988; Vogel and Garlick 1970).

Taking into account either of the two main models for TTG formation: partial melting of oceanic crust during subduction or anatexis of thickened lower crust in the roots of oceanic plateaus (Zhang et al. 2009), a limited contribution of crustal material is typically expected (Condie 2013). This is consistent with the $\delta^{18}O$ values previously recorded in TTGs and adakites, which range from 5.4 ± 0.3‰ (King et al. 2000) to above the mantle values 7.1–8.3‰ (Bindeman et al. 2005; Faure and Harris 1991; Whalen et al. 2002). If mantle eclogites were melt residues from Archaean crust formation, they would have $\delta^{18}O$ values that are only slightly lower (< 0.4‰, Korolev et al. 2018), as a function of the degree of melt produced and extracted and of the modal abundance of omphacite and garnet (i.e., increasing melt fraction leads to a progressively ^{18}O-enriched residue), with modelled values in the range of 5.2–5.8‰ (Bindeman et al. 2005). Therefore, the TTG residue model fails to account for the variability in $\delta^{18}O$ values of our mantle eclogites

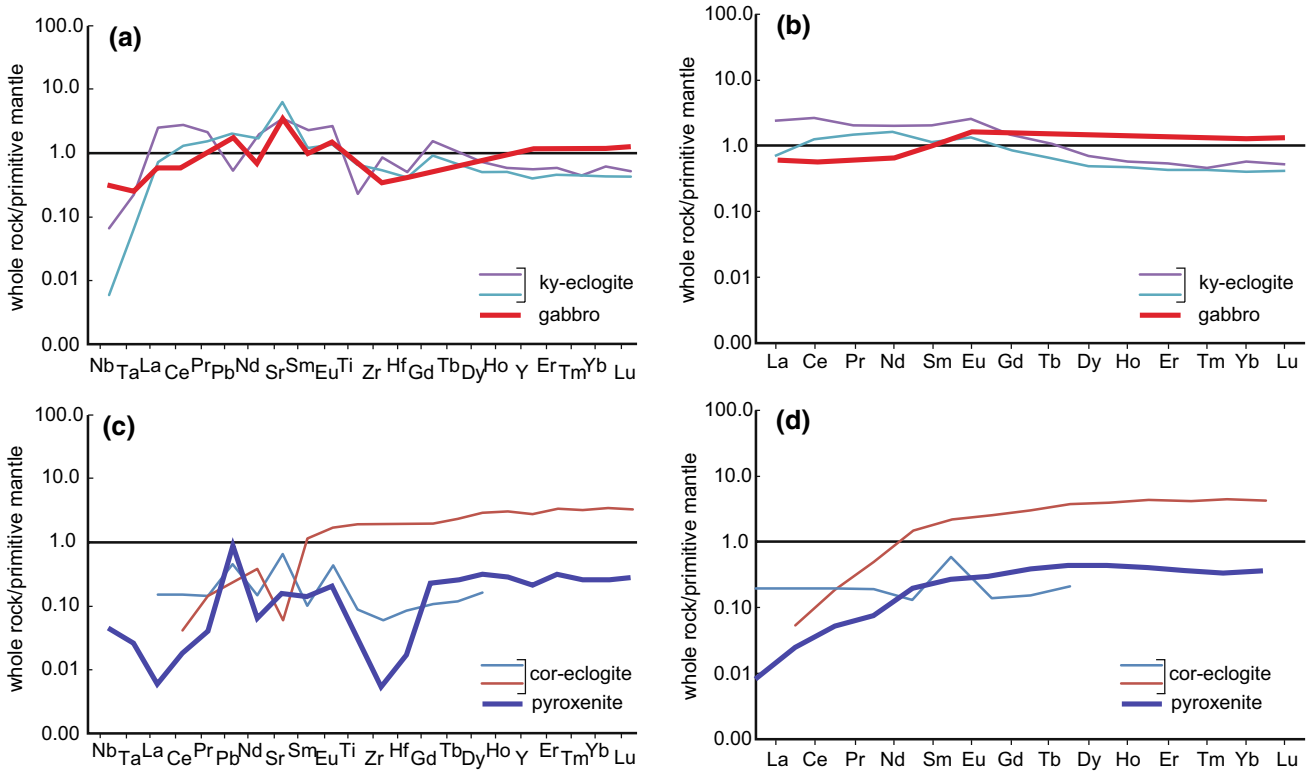

Fig. 13 Reconstructed whole-rock REE and extended trace elements patterns in kyanite-(**a, b**) and corundum-bearing eclogites (**c, d**) from the Kaapvaal craton, compared to the composition of gabbro and pyroxenite, respectively (GEOROC compilation)

(Table 1) and, in particular the $\delta^{18}O$ values that are lower than the peridotitic mantle.

Estimated bulk rock $\delta^{18}O$ values are between 5.6 and 6.7‰ for kyanite-bearing eclogites and between 1.4 and 4.8‰ for corundum-bearing eclogites. Compared to bimineralic eclogites, kyanite-bearing eclogites are interpreted to be derived from oceanic crust whose upper part underwent isotopic exchange during low-temperature alteration (Eiler 2001; Garlick et al. 1971; Schulze et al. 2013), and corundum-bearing eclogites are interpreted to be derived from the lower section of an oceanic crust that was subjected to high-temperature alteration (McCulloch et al. 1981; Shervais et al. 1988; Vogel and Garlick 1970). The garnet $\delta^{18}O$ values of 1.1‰ ($n=4$, $1\sigma=0.22$) in one of the corundum eclogites is significantly lower than any other $\delta^{18}O$ values previously measured in Phanerozoic ophiolites. There are several possible explanations for these low-$\delta^{18}O$ values. (1) They could be preserved from an oceanic crust derived from an Archaean mantle having lower $\delta^{18}O$ values than its more modern counterparts; this is supported by a recent study on Archaean komatiites from Barberton where, based on $\delta^{18}O$ values of fresh olivine crystals, it was inferred that mantle-derived magmas in the Archaean had significantly lower $\delta^{18}O$ values than the mantle today [3.5 ± 0.6‰ Byerly et al. (2017)]. (2) Low-$\delta^{18}O$ values recorded in this study could be explained if the seawater involved in the alteration had lower $\delta^{18}O$ values than the seawater that infiltrated Phanerozoic ophiolites (Gregory and Taylor 1981). (3) Alteration could have taken place at higher temperatures than in the case of Phanerozoic ophiolites, leading to a smaller rock-water oxygen fractionation. This will be discussed further below.

Influence of mantle metasomatism on $\delta^{18}O$

Some authors have put forward a metasomatic origin for $\delta^{18}O$ in eclogite xenoliths caused by interaction with carbonaceous, hydrous melts or fluids (Gréau et al. 2011; Huang et al. 2012). This model, is based on intra-sample variability in garnet $\delta^{18}O$ value, correlating with tracers of metasomatism (i.e., LREE, HFSE, Sr, etc.), and decoupling between the oxygen and magnesium isotope composition (Huang et al. 2016).

There are several issues concerning the metasomatic interpretation of oxygen isotope values in mantle eclogites that we will address point by point. First, no variability between mineral replicates and no correlation between typical metasomatic indicators (e.g., LREE, Hf, Zr) and $\delta^{18}O$ values are observed in the extended set of non-metasomatized eclogites from this study, where both lower and higher $\delta^{18}O$ values with respect to 'normal' mantle are

present. Second, according to a recent study of both oxygen and magnesium isotopes in mantle eclogites (Huang et al. 2016), the variable δ^{26}Mg (−1.09 to −0.17‰) with constant δ^{18}O values (2.34–2.91‰) are interpreted as evidence for a metasomatism arguing that they could not be inherited from an altered oceanic crustal protolith. However, studies on both continental (Li et al. 2011; Wang et al. 2014) and cratonic eclogites (Wang et al. 2012) show that a wide range of δ^{26}Mg values (−1.38 to +0.17‰, Wang et al. 2015) can be inherited from an oceanic crust which underwent hydrothermal alteration prior to subduction.

Moreover, a link between low-δ^{18}O values (< 5‰) and mantle metasomatism is inherently unlikely for reasons of mass balance. Oxygen is the most abundant element in mantle rock forming minerals (about 45% by weight). In this case, even a small (i.e., < 1‰) change in the oxygen isotopic ratio of mantle eclogites, with respect to the 'normal' mantle values [+5.5 ± 0.4‰ Mattey et al. (1994)] would require substantial amounts of fluids with unrealistically low-δ^{18}O values (Ionov et al. 1994; Riches et al. 2016a). Mass balance calculations for a volumetrically significant reactive agent that could change δ^{18}O values in eclogites without equilibrating with the surrounding mantle shows that a 1‰ change requires a maintained continuous flow from the source and across the upper mantle, of a fluid extremely different in δ^{18}O values, at a ≥ 2:5 fluid–rock ratio (Riches et al. 2016a). A metasomatic agent with extremely low-δ^{18}O values, overprinting the lower part of the cratonic root, without re-equilibrating with the surrounding peridotitic mantle seems unlikely and any mantle metasomatic agent is predicted to either shift the δ^{18}O values towards mantle-like values or have a negligible contribution (Aulbach et al. 2017b; Czas 2018). We, therefore, infer that oxygen isotope signature measured in eclogite xenoliths does not have a mantle source.

Origin of oxygen isotope variations in the protolith

Oxygen isotope ratios in mafic rocks may vary with respect to 'normal' mantle values as a result of fluid–rock interaction at variable temperature and crustal contamination. The δ^{18}O values of the eclogitic garnets from Roberts Victor vary from 1.1‰ to 7.4‰. This partly overlaps previously documented δ^{18}O values in eclogite suites worldwide (Beard et al. 1996; Caporuscio 1990; Garlick et al. 1971; Gréau et al. 2011; Huang et al. 2014, 2016; Jagoutz et al. 1984; MacGregor and Manton 1986; Neal et al. 1990; Ongley et al. 1987; Riches et al. 2016b; Schulze et al. 2000; Shervais et al. 1988; Sommer et al. 2017) (Fig. 14) and includes values that are lower than those previously measured. Bimineralic eclogites have "typical" δ^{18}O values according to the majority of the eclogites previously documented (Fig. 15a–c). Nevertheless, most of the oxygen isotope database on mantle eclogites from the Kaapvaal craton seems to be on metasomatized eclogites, based on their given textures or high alkali content. Conversely, pristine eclogites have been significantly less documented due to their low abundance. Unlike Type I eclogites that typically have mantle or higher than mantle δ^{18}O values, pristine Type II eclogites have lower values (with ~ 77% of δ^{18}O in garnet < 5‰).

As previously discussed, the non-metasomatized high Mg, Type IIA, eclogites characterized by lower equilibrium temperatures have a wide range in δ^{18}O values, from lower to higher than the 'normal' mantle, whereas Type IIB eclogites, with a low-Mg content and high equilibrium temperatures always have lower δ^{18}O values (Fig. 15d). Kyanite-bearing eclogites have δ^{18}O values within or above the 'normal' mantle range, similar to Type IIA eclogites, whereas the corundum-bearing samples have lower δ^{18}O values than peridotitic mantle. Sample RV344 has average garnet δ^{18}O values of 1.1‰ ($n = 4$, $1\sigma = 0.2$), ~ 1‰ lower than any previously recorded value in mantle eclogites (2.20‰ MacGregor and Manton 1986).

The variation in δ^{18}O values cannot be accounted for by fractionation under high-temperature mantle conditions (Bindeman 2008 and references therein; Shervais et al. 1988) and are, therefore, not consistent with a mantle origin for eclogite xenoliths that does not involve crustal recycling. It is inferred the bulk eclogite δ^{18}O values we estimated most likely reflect the range of δ^{18}O values of a subducted oceanic crust profile. Taking into account that low-δ^{18}O values are typically restricted to the lower segment of the oceanic crust

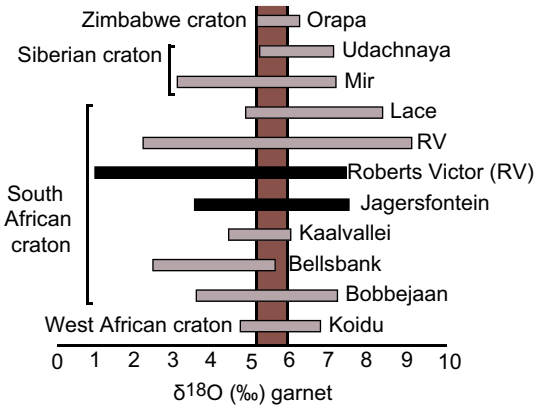

Fig. 14 Oxygen isotope compositions of eclogite garnets from Jagersfontein and Roberts Victor mines analyzed in this study (black bars) and literature data from worldwide eclogite suites (pink bars): Orapa (Aulbach et al. 2017a); Udachnaya (Jacob et al. 1994; Shatsky et al. 2016); Mir (Beard et al. 1996); Lace (Aulbach et al. 2017b); Roberts Victor (Garlick et al. 1971; Jagoutz et al. 1984; Ongley et al. 1987; MacGregor and Manton 1986; Caporuscio 1990; Schulze et al. 2000; Gréau et al. 2011; Huang et al. 2014, 2016; Riches et al. 2016a, b); Kaalvallei (Viljoen et al. 2005); Bellsbank (Neal et al. 1990; Shervais et al. 1988); Bobbejaan (Caporuscio 1990); Koidu (Barth et al. 2001, 2002)

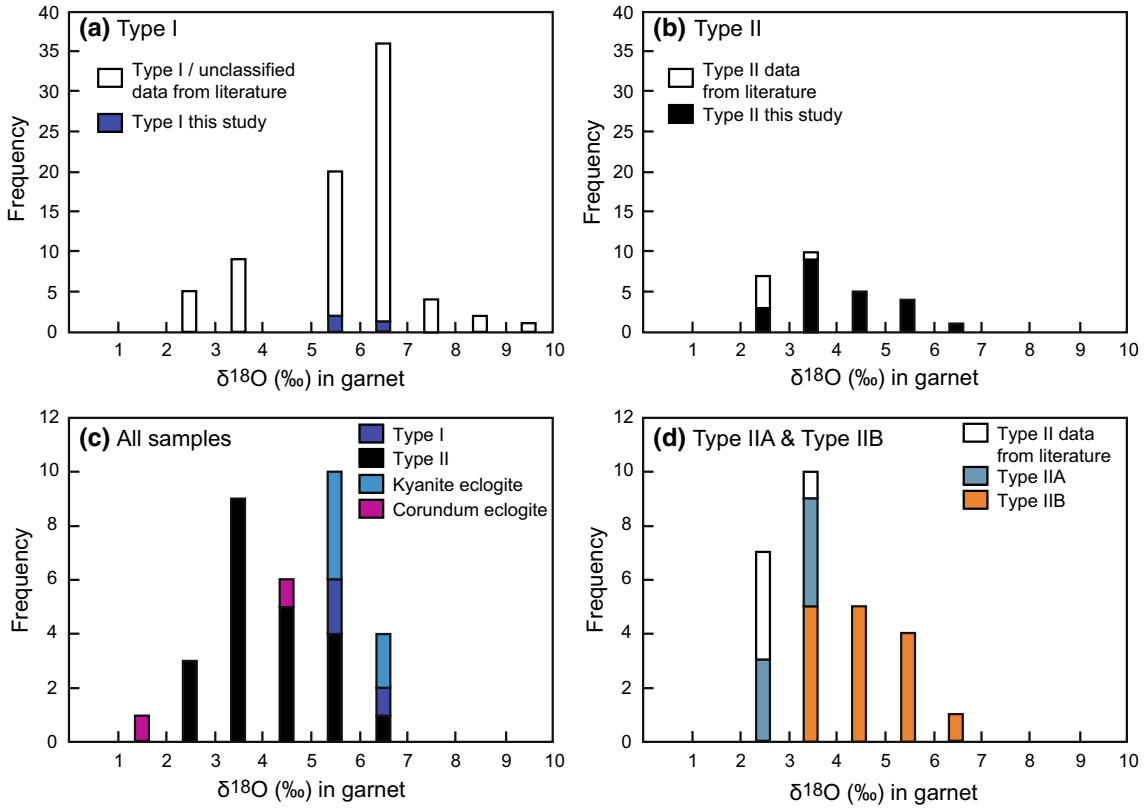

Fig. 15 Histograms showing oxygen isotope compositions of garnets from Roberts Victor mine from this study, compared to literature data from: Caporuscio (1990); Garlick et al. (1971); Gréau et al. (2011); Huang et al. (2014, 2016); Jagoutz et al. (1984); MacGregor and Manton (1986); Ongley et al. (1987); Riches et al. (2016a, b); Schulze et al. (2000), in **a** Type I (metasomatized) eclogites; **b** in Type II (non-metasomatized) eclogites; **c** in Type II (black), Type I eclogites (dark blue), kyanite- (light blue) and corundum-bearing (violet) eclogite xenoliths; **d** in bimineralic Type IIA (high Mg) and Type IIB (low Mg) eclogites

and high-$\delta^{18}O$ values to the upper section (Gregory and Taylor 1981), it is unclear if the two eclogite types (i.e. IIA; IIB) are derived from different parts of the same oceanic crust (i.e., ~ 150 km; ~ 210 km) or are derived from oceanic crust subducted at different times. Korolev et al. (2018) quantified the effects of typical processes associated with subduction (i.e., dehydration, partial melting, exogenous fluid flux, and progressive garnet overgrowth) on $\delta^{18}O$ values to be less than 1‰ individually or ~ 2.5‰ a possible total contribution; and of local mantle metasomatism as typically no more than 1–1.2‰. Nevertheless, the effects of metasomatism are strongly dependant on the difference between the initial rock composition and the $\delta^{18}O$ values of the metasomatic agent. It is, therefore, possible that the initial composition of the protolith has been slightly affected during subduction and concurrent metamorphism, nevertheless this excludes a mantle origin for the $\delta^{18}O$ values measured.

The $\delta^{18}O$ values recorded in our samples extend at least 2‰ lower than $\delta^{18}O$ values previously obtained from Cretaceous ophiolites (Alt and Bach 2006; Gregory and Taylor 1981). To produce $\delta^{18}O$ values as low as ~ 1‰ in the Phanerozoic (assuming a $\delta^{18}O$ value of seawater = 0‰), seawater–rock interactions would require either higher water to rock ratio or higher temperatures than envisaged for the Cretaceous ophiolites, which seem improbable (Kastings et al. 2006 and references therein). Most of the oxygen budget on Earth is contained in silicate minerals in the crust and mantle (Walker and Lohmann 1989) and the oxygen isotope record of the hydrosphere is controlled by the exchange of oxygen with silicate rocks (Perry and Ahmad 1983). Although in a recent study on Archaean komatiites, the $\delta^{18}O$ values of olivine phenocrysts from Barberton (3.5 ± 0.6‰) are interpreted as evidence for lower $\delta^{18}O$ values in the bulk Archaean mantle (Byerly et al. 2017), this seems unlikely to be the general case on the grounds of mass balance, as there is no evidence for a $\delta^{18}O$-enriched, unaltered Archaean oceanic crust. This is further supported by $\delta^{18}O$ values in Archaean eclogite xenoliths (e.g., Aulbach et al. 2017a, b; Jacob 2004; Korolev et al. 2018 and references therein) and eclogitic inclusions in diamonds (Deines et al. 1991) that overlap with the 'normal' modern mantle range.

Conversely, in the context of a mantle with higher heat-flow the associated oceanic crust is expected to be thicker and more buoyant (Bickle 1986; Smithies et al. 2003). The

equivalent of modern high-temperature hydrothermal systems found at axial mid-ocean ridges, might, therefore, be restricted to shallower depths (Kastings et al. 2006). In such a system with less effective fluid circulation, low-temperature oxygen isotope exchange is expected to dominate, generating lower seawater $\delta^{18}O$ values (Kastings et al. 2006; Walker and Lohmann 1989). At the same time, enhanced continental weathering due to higher pCO_2 levels and the presence of extensive greenstone belts (areas of high low-temperature hydrothermal alteration De Wit et al. 1982) are believed to have had a significant contribution in the low-$\delta^{18}O$ values of Archaean seawater (Jaffres et al. 2007; Walker and Lohmann 1989). This is supported by oxygen isotope variations recorded in (bio)chemical marine sedimentary rocks, such as chert and calcite, indicating seawater had lower $\delta^{18}O$ values in the past, estimated at ~ − 10‰ in the Archaean, compared to present values (~ 0.00‰ SMOW) (Burdett et al. 1990; Hren et al. 2009; Jaffres et al. 2007; Veizer and Prokoph 2015; Walker and Lohmann 1989). Although Archaean seawater temperature may have been higher, leading to lower $\delta^{18}O$ values of altered oceanic crust (Jaffres et al. 2007 and references therein) it cannot be the only explanation for the $\delta^{18}O$ values recorded in some of our samples or in some Archaean sedimentary rocks (~ 8‰ lower than modern carbonates, Kastings et al. 2006; Knauth and Lowe 1978, 2003; Veizer et al. 1999). In conclusion, the low-$\delta^{18}O$ values measured in the Kaapvaal eclogites from this study are most likely the result of the interaction of an oceanic crustal protolith with Archaean seawater that had lower $\delta^{18}O$ value than present as suggested by Kastings et al. (2006) and references therein.

Conclusions

1. The correlation between garnet and clinopyroxene $\delta^{18}O$ values ($r^2 = 0.98$) and the constant Δ_{cpx-gt} (− 0.22 to + 0.31‰, $n = 35$), Δ_{gt-ky} (− 0.37 to − 0.30‰, $n = 3$) and Δ_{gt-cor} (+ 0.05 to + 0.31‰, $n = 4$) among the minerals present in each of our samples are evidence for oxygen isotope equilibrium at mantle temperatures. We, therefore, conclude that the whole rock $\delta^{18}O$ values estimated in this work for eclogite xenoliths, were most likely inherited from their protolith.
2. Bimineralic eclogites from the Kaapvaal craton, showing little or no signs of kimberlite metasomatism, can be defined as high-magnesium (Type IIA) and low-magnesium (Type IIB) eclogites. Based on reconstructed whole-rock major and trace element compositions and oxygen isotope ratios, both compositional types are interpreted to be derived from an Archaean oceanic crust formed from an evolved picritic liquid. The wide range in $\delta^{18}O$ values (1.1–7.6‰) present in samples with a narrow major and trace element compositional range is interpreted as being caused by hydrothermal alteration of the ocean crust at variable temperatures. Type IIB eclogites were sampled from greater depths (~ 160–240 km) than Type IIA (~ 70–160 km), and suffered a small degree of melt loss before or during eclogitization. It is unclear whether both types are derived from the same oceanic crust, or from ocean crust recycled at different times.
3. Our non-metasomatized eclogites predominantly have estimated bulk $\delta^{18}O$ values that are lower than asthenospheric mantle and one corundum-bearing eclogite from Roberts Victor has bulk $\delta^{18}O$ values of 1.4‰ which is the lowest so far measured in mantle eclogites. A mantle metasomatic agent with extremely low-$\delta^{18}O$ values overprinting the lower part of the cratonic root before the kimberlite eruption, without re-equilibrating with the surrounding peridotitic mantle is considered unlikely. It is more likely that oxygen isotope ratios in non-metasomatized eclogites are inherited from the ancient protolith.
4. Kyanite-bearing eclogites have positive Sr and Eu anomalies and, based on reconstructed whole-rock compositions, are interpreted to be derived from a gabbroic protolith, whereas corundum-bearing eclogites were derived from a pyroxene-dominated crustal cumulate.
5. Assuming our data represent a profile through oceanic crust that has its lowest $\delta^{18}O$ values ~ 2‰ lower than profiles reconstructed from Cretaceous ophiolites, this is most probably the result of interaction with Archaean seawater having lower $\delta^{18}O$ values, perhaps combined with a higher thermal regime for seawater–rock interaction.

Acknowledgements We are grateful to J.L. Devidal for his assistance with the electron microprobe and LA-ICP-MS analyses and to Sherissa Roopnarain for the mass spectrometer analyses. D. Jacob, F. Viljoen and M. Grégoire are gratefully acknowledged for improving an earlier version of this manuscript as part of IBR's PhD thesis. We are equally grateful for the opportunity to use the JXA8230 EPMA at Rhodes University. The financial support from Jean Monnet University of Saint Etienne, through doctoral scholarship and international travel grants and from the National Research Foundation (South Africa) are hereby acknowledged. This research has been equally made possible through the financial support from the French Government Laboratory of Excellence initiative n° ANR-10-LABX-0006, the Region Auvergne and the European Regional Development Fund. This is Laboratory of Excellence ClerVolc contribution number 334. We are thankful to Sonja Aulbach and Dorrit Jacob for their constructive comments that helped to considerably improve the manuscript.

References

Agashev AM, Pokhilenko LN, Pokhilenko NP, Shuchukina EV (2018) Geochemistry of eclogite xenoliths from the Udachnaya Kimberlite Pipe: section of ancient oceanic crust sampled. Lithos 314–315:187–200 https://doi.org/10.1016/j.lithos.2018.05.027

Alt JC, Bach W (2006) Oxygen isotopic composition of a section of lower oceanic crust, ODP Hole 735B. Geochem Geophys Geosyst. https://doi.org/10.1029/2006GC001385

Ater PC, Eggler DH, McCallum ME (1984) Petrology and geochemistry of mantle eclogite xenoliths from Colorado–Wyoming kimberlites: recycled ocean crust? In: J. K-P (ed) Kimberlites II: the mantle and the crust–mantle relationships. Elsevier, Amsterdam, pp 309–318

Aulbach S (2012) Craton nucleation and formation of thick lithospheric roots. Lithos 149:16–30. https://doi.org/10.1016/j.lithos.2012.02.011

Aulbach S, Jacob DE (2016) Major- and trace-elements in cratonic mantle eclogites and pyroxenites reveal heterogeneous sources and metamorphic processing of low-pressure protoliths. Lithos 262:586–605. https://doi.org/10.1016/j.lithos.2016.07.026

Aulbach S, Viljoen KS (2015) Eclogite xenoliths from the Lace kimberlite, Kaapvaal craton: from convecting mantle source to palaeo-ocean floor and back. Earth Planet Sci Lett 431:274–286. https://doi.org/10.1016/j.epsl.2015.08.039

Aulbach S, Shirey SB, Stached T, Creighton S, Muehlenbachs K, Harris JW (2009) Diamond formation episodes at the southern margin of the Kaapvaal Craton: Re–Os systematics of sulfide inclusions from the Jagersfontein Mine. Contrib Miner Petrol 157:525–540. https://doi.org/10.1007/s00410-008-0350-9

Aulbach S, O'Reilly SY, Pearson NJ (2011) Constraints from eclogite and MARID xenoliths on origins of mantle Zr/Hf–Nb/Ta variability. Contrib Miner Petrol 162:1047–1062. https://doi.org/10.1007/s00410-011-0639-y

Aulbach S, Gerdes A, Viljoen KS (2016) Formation of diamondiferous kyanite-eclogite in a subduction mélange. Geochim Cosmochim Acta 179:156–176. https://doi.org/10.1016/j.gca.2016.01.038

Aulbach S, Jacob DE, Cartigny P, Stern RA, Simonetti SS, Wörner G, Viljoen KS (2017a) Eclogite xenoliths from Orapa: Ocean crust recycling, mantle metasomatism and carbon cycling at the western Zimbabwe craton margin. Geochim Cosmochim Acta 213:574–592. https://doi.org/10.1016/j.gca.2017.06.038

Aulbach S, Woodland AB, Vasilyev P, Galvez ME, Viljoen KS (2017b) Effects of low-pressure igneous processes and subduction on Fe3+/ΣFe and redox state of mantle eclogites from Lace (Kaapvaal craton). Earth Planet Sci Letters 474:283–295. https://doi.org/10.1016/j.epsl.2017.06.030

Barth MG, Rudnick RL, Horn I, McDonough WF, Spicuzza MJ, Valley J, Haggerty SE (2001) Geochemistry of xenolithic eclogites from West Africa, Part I: a link between low MgO eclogites and Archean crust formation. Geochim Cosmochim Acta 65:1499–1527. https://doi.org/10.1016/S0016-7037(00)00626-8

Barth MG, Rudnick RL, Horn I, McDonough WF, Spicuzza MJ, Valley JW, Haggerty SE (2002) Geochemistry of xenolithic eclogites from West Africa, part 2: Origins of the high MgO eclogites. Geochim Cosmochim Acta 66:4325–4345. https://doi.org/10.1016/S0016-7037(02)01004-9

Beard BL, Fraracci KN, Taylor LA, Snyder GA, Clayton RN, Mayeda TK, Sobolev NV (1996) Petrography and geochemistry of eclogites from the Mir kimberlite, Yakutia, Russia. Contrib Miner Petrol 125:293–310. https://doi.org/10.1007/s004100050

Bickle MJ (1986) Implications of melting for stabilisation of the lithosphere and heat loss in the Archaean. Earth Planet Sci Lett 80:314–324. https://doi.org/10.1016/0012-821X(86)90113-5

Bindeman I (2008) Oxygen isotopes in mantle and crustal magmas as revealed by single crystal. Analysis Rev Mineral Geochem 69:445–478

Bindeman IN et al (2005) Oxygen isotope evidence for slab melting in modern and ancient subduction zones. Earth Planet Sci Lett 235:480–496. https://doi.org/10.1016/j.epsl.2005.04.014

Bowers TS, Taylor HP Jr (1985) An integrated chemical and stable-isotope model of the origin of Midocean Ridge hot spring systems. J Geophys Res Solid Earth 90:12583–12606. https://doi.org/10.1029/JB090iB14p12583

Burdett JW, Grotzinger JP, Arthur MA (1990) Did major changes in the stable-isotope composition of Proterozoic seawater occur? Geology 18:227–230 https://doi.org/10.1130/0091-7613(1990)018%3C0227:DMCITS%3E2.3.CO;2

Byerly BL, Kareem K, Bao H, Byerly GR (2017) Early Earth mantle heterogeneity revealed by light oxygen isotopes of Archean komatiites Nat Geosci 1–5

Caporuscio FA (1990) Oxygen isotope systematics of eclogite mineral phases from South Africa. Lithos 203–210

Caporuscio FA, Smyth JR (1990) Trace elements crystal chemistry of mantle eclogites. Contrib Miner Petrol 105:550–561. https://doi.org/10.1007/BF00302494

Clark JR, Papike JJ (1968) Crustal-chemical characterization of omphacites. Am Miner 53:840–868

Condie KC (2013) Evolution of Archean crust and early life vol 7. Modern approaches in solid earth sciences. Springer

Czas J (2018) The quandary of the Sask Craton: origin and evolution of the lithospheric mantle beneath the Sask Craton. University of Alberta

De Wit MJ, Hart R, Martin A, Abbott P (1982) Archean abiogenic and probable biogenic structures associated with mineralized hydrothermal vent systems and regional metasomatism, with implications for greenstone belt studies. Econ Geol 77:1783–1802. https://doi.org/10.2113/gsecongeo.77.8.1783

de Wit MJ et al (1992) Formation of an Archean continent. Nature 357:553–562

Deines P, Harris JW, Robinson DN, Gurney JJ, Shee SR (1991) Carbon and oxygen isotope variations in diamond and graphite eclogites from Orapa, Botswana, and the nitrogen content of their diamonds. Geochim Cosmochim Acta 55:515–524. https://doi.org/10.1016/0016-7037(91)90009-T

Eiler JM (2001) Oxygen isotope variations of basaltic lavas and upper mantle rocks. Rev Miner Geochem 43:319–364

Faure K, Harris C (1991) Oxygen and carbon isotope geochemistry of the 3.2 Ga Kaap Valley tonalite, Barberton greenstone belt, South Africa. Precambrian Res 301–319

Field M, Stiefenhofer J, Robey J, Kurszlaukis S (2008) Kimberlite-hosted diamond deposits of southern Africa: a review. Ore Geol Rev 33–75

Garber JM et al (2018) Multidisciplinary constraints on the abundance of diamond and eclogite in the cratonic lithosphere. Geochem Geophys Geosyst 19:2062–2086. https://doi.org/10.1029/2018GC007534

Garlick GD, MacGregor ID, Vogel DE (1971) Oxygen isotope ratios in eclogites from kimberlites. Science 172:1025–1027

Gonzaga RG, Menzies MA, Thirlwall MF, Jacob DE, Leroex A (2010) Eclogites and garnet pyroxenites: problems resolving provenance using Lu-Hf, Sm-Nd and Rb-Sr isotope systems. J Petrol 51:513–535. https://doi.org/10.1093/petrology/egp091

Gréau Y, Huang J-X, Griffin WL, Renac C, Alard O, O'Reilly SY (2011) Type I eclogites from Roberts Victor kimberlites: products of extensive mantle metasomatism. Geochim Cosmochim Acta 75:6927–6954. https://doi.org/10.1016/j.gca.2011.08.035

Gregory RT, Taylor HP (1981) An oxygen isotope profile in a section of cretaceous oceanic crust, Samail Ophiolite, Oman: evidence from d18O buffering in the oceans by deep (> 5 km)

seawater–hydrothermal circulation at mid-ocean ridges. J Geophys Res Solid Earth 86:2737–2755. https://doi.org/10.1029/JB086iB04p02737
Griffin WL, O'Reilly SY (2007) Cratonic lithospheric mantle: Is there anything subducted? Episodes 30:43–53
Griffin W, O'Reilly SY, Natapov LM, Ryan CG (2003) The evolution of the lithospheric mantle beneath the Kalahari craton and its margins. Lithos 71:215–241
Haggerty SE, Sautter V (1990) Ultradeep (Greater than 300 kilometers). Ultramafic upper mantle xenoliths. Science 248:993–996
Harris C, Vogeli J (2010) Oxygen isotope composition of garnet in the peninsula granite, cape granite suite, South Africa: constraints on melting and emplacement mechanisms South African. J Geol 113:385–396
Harte B, Gurney J (1975) Evolution of clinopyroxene and garnet in an eclogite nodule from the Roberts Victor kimberlite pipe, S Afr Phys Chem Earth:367–387
Harte B, Kirkley MB (1997) Partitioning of trace elements between clinopyroxene and garnet: data from mantle eclogites. Chem Geol 136:1–24. https://doi.org/10.1016/S0009-2541(96)00127-1
Hatton CJ (1978) The geochemistry and origin of xenoliths from the Roberts Victor mine. University of Cape Town, CT
Hatton CJ, Gurney J (1977) Igneous fractionation trends in Roberts-Victor eclogites. Paper presented at the 2nd International Kimberlite Conference
Helmstaedt H, Doig R (1975) Eclogite nodules from kimberlite pipes of the Colorado plateau—samples of subducted francinsca-type oceanic lithosphere. Phys Chem Earth 9:95–112
Herzberg C (2011) Basalts as temperature probes of Earth's mantle. Geology 39:1179–1180. https://doi.org/10.1130/focus122011.1
Herzberg C, O'Hara MJ (1998) Phase equilibrium constraints on the origin of basalts, picrites, and komatiites. Earth Sci Rev 44:39–79. https://doi.org/10.1016/S0012-8252(98)00021-X
Howarth GH et al (2014) Superplume metasomatism: Evidence from Siberian matle xenoliths Lithos:209–224
Hren MT, Tice MM, Chamberlain CP (2009) Oxygen and hydrogen isotope evidence for a temperate climate 3.42 billion. years ago Nature 462:205. https://doi.org/10.1038/nature08518
Huang J-X, Gréau Y, Griffin WL, O'Reilly SY, Pearson NJ (2012) Multi-stage origin of Roberts Victor eclogites: progressive metasomatism and its isotopic effects. Lithos 161–181
Huang J-X, Griffin WL, Gréau Y, Pearson NJ, O'Reilly SY, Cliff J, Martin L (2014) Unmasking xenolithic eclogites: progressive metasomatism of a key Roberts Victor sample. Chem Geol 364:56–65. https://doi.org/10.1016/j.chemgeo.2013.11.025
Huang J-X et al (2016) Magnesium and oxygen isotopes in Roberts Victor eclogites. Chem Geol 438:73–83. https://doi.org/10.1016/j.chemgeo.2016.05.030
Ionov DA, Harmon RS, France-Lanord C, Greenwood PB, Ashchepkovm IV (1994) Oxygen isotope composition of garnet and spinel peridotites in the continental mantle: evidence from the Vitim xenoltih suite, southern Siberia. Geochim Cosmochim Acta 58:1463–1470. https://doi.org/10.1016/0016-7037(94)90549-5
Ireland TR, Rudnick RL, Spetsius ZV (1994) Trace elements in diamond inclusions from eclogites reveal link to Archean granites Earth Planet Sci Lett 128 https://doi.org/10.1016/0012-821X(94)90145-7
Jacob DE (2004) Nature and origin of eclogite xenoliths from kimberlites. Lithos 295–316
Jacob DE, Foley SF (1999) Evidence for Archean ocean crust with low high field strength element signature from diamondiferous eclogite xenoliths. Lithos 317–336
Jacob DE, Jagoutz E, Lowry D, Mattey D, Kudrjavttseva G (1994) Diamondiferous eclogites from Siberia: remnants of Archean oceanic crust. Geochim Cosmochim Acta 58:5191–5207. https://doi.org/10.1016/0016-7037(94)90304-2
Jacob DE, Schmickler B, Schulze DJ (2003) Trace element geochemistry of coesite-bearing eclogites from the Roberts Victor kimberlite, Kaapvaal craton. Lithos 337–351
Jacob DE, Bizimis M, Salters VJM (2005) Lu-Hf and geochemical systematics of recycled ancient oceanic crust: evidence from Roberts Victor eclogites. Contrib Miner Petrol 148:707–720. https://doi.org/10.1007/s00410-004-0631-x
Jaffres BDJ, Shields GA, Wallmann K (2007) The oxygen isotope evolution of seawater: a critical review of a long-standing controversy and an improved geological water cycle mode for the past 3.4 billion years. Earth Sci Rev 83:83–122. https://doi.org/10.1016/j.earscirev.2007.04.002
Jagoutz E, Dawson JB, Hoernes S, Spettel B, Wänke H (1984) Anorthositic oceanic crust in the Archean. Earth Lunar Planet Sci 15:395–396
James DE, Niu F, Rokosky J (2003) Crustal structure of the Kaapvaal craton and its significance for early crustal evolution. Lithos 413–429
Kastings FJ, Tazewell Howard M, Wallmann K, Veizer J, Shields G, Jaffres J (2006) Paleoclimates, ocean depth, and the oxygen isotopic composition of seawater. Earth Planet Sci Lett 252:82–93. https://doi.org/10.1016/j.epsl.2006.09.029
Katayama I, Suyama Y, Ando J, Komiya T (2009) Mineral chemistry and P-T condition of granular and sheared peridotite xenoliths from Kimberley, South Africa: Origin of the textural variation in the cratonic mantle. Lithos 109(3–4):333–340
King EM, Valley JW, Davis DW (2000) Oxygen isotope evolution of volcanic rocks at the Sturgeon Lake volcanic complex, Ontario. Can J Earth Sci 37:39–50. https://doi.org/10.1139/e99-106
Knauth LP, Lowe DR (1978) Oxygen isotope geochemistry of cherts from the Onverwacht group (3.4 billion years), Transvaal, South Africa, with implications for secular variations in the isotopic composition of cherts. Earth Planet Sci Lett 41:209–222. https://doi.org/10.1016/0012-821X(78)90011-0
Knauth LP, Lowe DR (2003) High Archean climatic temperature inferred from oxygen isotope geochemistry of cherts in the 3.5 Ga Swaziland Supergroup, South Africa. Geol Soc Am Bull 115:566–580 https://doi.org/10.1130/0016-7606(2003)115%3C0566:HACTIF%3E2.0.CO;2
Korolev NM, Melnik AE, Li X-H, Skublov SG (2018) The oxygen isotope composition of mantle eclogites as a proxy of their origin and evolution: a review. Earth Sci Rev 185:288–300. https://doi.org/10.1016/j.earscirev.2018.06.007
Krogh E (1988) The garnet-clinopyroxene Fe–Mg geothermometer—a reinterpretation of existing experimental data. Contrib Miner Petrol 99:44–48. https://doi.org/10.1007/BF00399364
Lappin MA (1978) The evolution of a grospydite from the Roberts Victor Mine, South Africa. Contrib Miner Petrol 66:229–241. https://doi.org/10.1007/BF00373407
Lappin MA, Dawson JB (1975) Two Roberts Victor cumulate eclogites and their re-equilibration. Phys Chem Earth 9:351–365
Li W-Y, Xiao F-ZT, Huang Y J (2011) High-temperature inter-mineral magnesium isotope fractionation in eclogite from the Dabie orogen China. Earth Planet Sci Lett 304:224–230. https://doi.org/10.1016/j.epsl.2011.01.035
MacGregor ID, Carter JL (1970) The chemistry of clinopyroxenes and garnets of eclogite and peridotite xenoliths from the Roberts Victor mine, South Africa. Phys Earth Planet Interiors 391–397
MacGregor ID, Manton WI (1986) Roberts Victor eclogites: ancient oceanic crust. J Geophys Res 91:14063–14079
Mattey D, Lowry D, Macpherson C (1994) Oxygen isotope composition of mantle peridotites. Earth Planet Sci Lett 128:231–241. https://doi.org/10.1016/0012-821X(94)90147-3
McCandless T, Gurney J (1989) Sodium in garnet and potassium in clinopyroxene: criteria for classifying mantle eclogites. In: Ross J, Jaques AL, Ferguson J, Green DH, O'Reilly SY, Danchin RV,

Janse AJA (eds) Kimberlite and related rocks. Special publication—Geological Society of Australia, Perth
McCulloch MT, Gregory RT, Wasserburg GJ, Taylor HP (1981) Sm-Nd, Rb-Sr and 18O/16O isotopic systematics in an oceanic crustal section: evidence from the samail ophiolite. J Geophys Res 86:2721–2735
McDonough WF, Sun S-S (1995) The composition of the. Earth Chem Geol 120:223–253. https://doi.org/10.1016/0009-2541(94)00140-4
McKenzie D, Bickle MJ (1988) The Volume and composition of melt generated by extension of the lithosphere. J Petrol 29:625–679. https://doi.org/10.1093/petrology/29.3.625
Misra KC, Anand M, Taylor LA, Sobolev NV (2004) Multi-stage metasomatism of diamondiferous eclogite xenoliths from the Udachnaya kimberlite pipe, Yakutia, Siberia. Contrib Miner Petrol 146:696–714. https://doi.org/10.1007/s00410-003-0529-z
Müller W, Shelley M, Miller P, Broude S (2009) Initial performance metrics of a new custom-designed ArF excimer LA-ICPMS system coupled to a two-volume laser-ablation cell. J Anal At Spectrom 24:209–214. https://doi.org/10.1039/B805995K
Neal CR et al (1990) Eclogites with oceanic crustal and mantle signatures from the Bellsbank kimberlite, South Africa, part 2: Sr, Nr and O istope geochemistry. Earth Planet Sci Lett 99:362–379
O'Hara MJ, Yoder JHS (1967) Formation and fractionation of basic magmas at high pressures. Scott J Geol 67–117
Ongley JS, Basu AR, Kyser KT (1987) Oxygen isotopes in coexisting garnets, clinopyroxenes and phlogopites of Roberts Victor eclogites: implications for petrogenesis and mantle metasomatism. Earth Planet Sci Lett 83:80–84. https://doi.org/10.1016/0012-821X(87)90052-5
Pearson DG (1999) The age of continental roots Lithos 48:171–194 https://doi.org/10.1016/S0024-4937(99)00026-2
Peck WH, Valley JW, Graham CM (2003) Slow oxygen diffusion rates in igneous zircons from metamorphic rocks. Am Miner 88:1003–1014. https://doi.org/10.2138/am-2003-0708
Perry ECJ, Ahmad SN (1983) Oxygen isotope geochemistry of Proterozoic chemical sediments. Geol Soc Am Memoir 161:253–264. https://doi.org/10.1130/MEM161-p253
Pollack HN, Chapman DS (1977) On the regional variations of the heat flow, geotherms, and lithospheric thickness. Tectonophysics 279–296
Pyle JM, Haggerty SE (1998) Eclogites and the metasomatism of eclogites from the Jagersfontein Kimberlite: punctuated transport and implications for alkali magmatism. Geochim Cosmochim Acta 62:1207–1231. https://doi.org/10.1016/S0016-7037(98)00040-4
Radu IB, Moine BN, Ionov DA, Korsakov A, Golovin AV, Mikhailenko D, Cottin J-Y (2017) Kyanite-bearing eclogite xenoliths from Udachnaya kimberlite, Siberian craton, Russia. Bull Soc Géol France 188:75–84. https://doi.org/10.1051/bsgf/2017008
Riches AJV et al (2016a) In situ oxygen-isotope, major-, and trace-element constraints on the metasomatic modification and crustal origin of a diamondiferous eclogite from Roberts Victor, Kaapvaal craton. Geochim Cosmochim Acta 174:345–359
Riches AJV et al (2016b) In situ oxygen-isotope, major-, and trace-element constraints on the metasomatic modification and crustal origin of a diamondiferous eclogite from Roberts Victor, Kaapvaal craton. Geochim Cosmochim Acta 174:345–359. https://doi.org/10.1016/j.gca.2015.11.028
Rollinson H (1997) Eclogite xenoliths in west African kimberlites as residues from Archean granitoid crust formation. Lett Nat 389:173–176
Schmickler B, Jacob DE, Foley SF (2004) Eclogite xenoliths from the Kuruman kimberlites, South Africa: geochemical fingerprinting of deep subduction and cumulate processes. Lithos 173–207
Schmitz MD, Bowring SA (2003) Ultrahigh-temperature metamorphism in the lower crust during Neoarchean Ventersdorp rifting and magmatism, Kaapvaal Craton, southern Africa. Geol Soc Am Bull 115:533–548 https://doi.org/10.1130/0016-7606(2003)115%3C0533:UMITLC%3E2.0.CO;2
Schroeder-Frerkes F, Woodland AB, Uenver-Thiele L, Klimm K, Knapp N (2016) Ca–Eskola incorporation in clinopyroxene: limitations and petrological implications for eclogites and related rocks. Contrib Miner Petrol. https://doi.org/10.1007/s00410-016-1311-3
Schulze DJ, Helmstaedt H (1988) Coesite-Sanidine eclogites from kimberlite: products of mantle fractionation or subduction? J Geol 96:435–443. https://doi.org/10.1086/629238
Schulze DJ, Valley J, Spicuzza MJ (2000) Coesite-sanidine eclogites from the Roberts Victor kimberlite, South Africa. Lithos 23–32
Schulze DJ, Harte B, staff EIMF, Zeb Page, Valley F, Channer JW, Jaques DMD AL (2013) Anticorrelation between low d13C of eclogitic diamonds and high d18O of their coesite and garnet inclusions requires a subduction origin. Geology 41:455–458. https://doi.org/10.1130/G33839.1
Shatsky VS, Zedgenizov DA, Ragozin AL (2016) Evidence for a subduction component in the diamond-bearing mantle of the Siberian craton. Russian Geol Geophys 57(1):111–126
Shchipansky AA (2012) Subduction geodynamics in Archean and formation of diamond-bearing lithospheric keels and early continental crust of cratons. Geotectonics 46:122–141. https://doi.org/10.1134/S0016852112020057
Shervais JW, Taylor LA, Lugmair GW, Clayton RN, Mayeda TK, Korotev RL (1988) Early Proterozoic oceanic crust and the evolution of subcontinental mantle: eclogites and related rocks from southern Africa. Bull Geol Soc Am 100:411–423 https://doi.org/10.1130/0016-7606(1988)100%3C0411:EPOCAT%3E2.3.CO;2
Shu Q, Brey GP, Hoefer HE, Zhao Z, Pearson DG (2016) Kyanite/corundum eclogites from the Kaapvaal Craton: subducted troctolites and layered gabbros from the Mid- to Early Archean. Contrib Miner Petrol. https://doi.org/10.1007/s00410-015-1225-5
Smith CB, Allsop HL, Kramers JD, Roddick JC (1985) Emplacement ages of Jurassic-Cretaceous South African kimberlites by the Rb–Sr method on phlogopite and whole-rock samples. Trans Geol Soc S Afr 88:249–266
Smithies RH, Champion D, Cassidy KF (2003) Formation of Earth's early Archaean continental crust. Precambrian Res 89–101
Smyth JR, Caporuscio FA (1984) Petrology of a suite of eclogite inclusions from the Bobbejaan kimberlite: II. Primary phase compositions and origin. In: Kornprobst J (ed) Kimberlites II: the mantle and crust–mantle relationship. Elsevier, Amsterdam, pp 121–131
Smyth JR, Caporuscio FA, McCormick TC (1989) Mantle eclogites: evidence of igneous fractionation in the mantle. Earth Planet Sci Lett 93:133–141. https://doi.org/10.1016/0012-821X(89)90191-X
Snyder GA, Jerde EA, Taylor LA, Halliday AN, Sobolev VN, Sobolev NV (1993) Nd and Sr isotopes from diamondiferous eclogites, Udachnaya Kimberlite Pipe, Yakutia, Siberia: evidence of differentiation in the early Earth? Earth Planet Sci Lett 118:91–100. https://doi.org/10.1016/0012-821X(93)90161-2
Sommer H, Jacob DE, Stern RA, Petts D, Mattey D, Pearson DG (2017) Fluid-induced transition from banded kyanite- to bimineralic eclogite and implications for the evolution of cratons. Geochim Cosmochim Acta 207:19–42. https://doi.org/10.1016/j.gca.2017.03.017
Taylor LA, Neal CR (1989) Eclogites with oceanic crustal and mantle signatures from the Bellsbank kimberlite, South Africa, Part I: Mineralogy, Petrography and whole rock chemistry J Geol:551–567
Van der Meer QHA, Klaver M, Waight TE, Davies GR (2013) The provenance of sub-cratonic mantle beneath the Limpopo Mobile Belt (South Africa). Lithos 170–171:90–104

van Reenen DD, Roering C, Ashwal LD, de Wit MJ (1992) Regional geological setting of the Limpopo Belt. Precambrian Res 55:1–5

van Achterbergh E, Ryan CG, Jackson SE, Griffin W (2001) Data reduction software for LA–ICP–MS. In Laser ablation-ICPMS in the earth science. In: Sylvester P (ed) Mineralogical association of Canada, vol 29. pp 239–243

Veizer J, Prokoph A (2015) Temperatures and oxygen isotopic composition of Phanerozoic oceans. Earth Sci Rev 146:92–104. https://doi.org/10.1016/j.earscirev.2015.03.008

Veizer J et al (1999) 87Sr/86Sr, d13C and d18O evolution of Phanerozoic seawater. Chem Geol 161:59–88

Viljoen KS, Schulze DJ, Quadling AG (2005) Contrasting Group I and Group II Eclogite Xenolith Petrogenesis: petrological, trace element and isotopic evidence from eclogite, garnet-websterite and alkremite xenoliths in the kaalvallei kimberlite, South Africa. J Petrol 46:2059–2090

Vogel DE, Garlick GD (1970) Oxygen-isotope ratios in metamorphic eclogites. Contrib Miner Petrol 28:183–191. https://doi.org/10.1007/BF00405748

Walker JCG, Lohmann KC (1989) Why the oxygen isotopic composition of sea water changes with time. Geophys Res Lett 16:323–326. https://doi.org/10.1029/GL016i004p00323

Wang S-J, Teng F-Z, Williams HM, Li S-G (2012) Magnesium isotopic variations in cratonic eclogites: origin and implications. Earth Planet Sci Lett 359–360:219–226. https://doi.org/10.1016/j.epsl.2012.10.016

Wang S-J, Fang-Zheng T, Li S-G, Hong J-A (2014) Magnesium isotopic systematics of mafic rocks during continental subduction. Geochim Cosmochim Acta 143:34–48. https://doi.org/10.1016/j.gca.2014.03.029

Wang S-J, Teng F-Z, Rudnick RL, Li S-G (2015) Magnesium isotope evidence for a recycled origin of cratonic eclogites. Geology 43:1071–1074. https://doi.org/10.1130/G37259.1

Whalen JB, Percival JA, McNicoll VJ, Longstaffe FJ (2002) A mainly crustal origin for tonalitic granitoid rocks, superior province, canada: implications for late Archean tectonomagmatic processes. J Petrol 43:1551–1570

Withers AC, Wood BJ, Carroll MR (1998) The OH content of pyrope at high pressure. Chem Geol 147:161–171. https://doi.org/10.1016/S0009-2541(97)00179-4

Zhang S-B, Zheng Y-F, Zhao Z-F, Wu Y-B, Yuan H, Wu F-Y (2009) Origin of TTG-like rocks from anatexis of ancient lower crust: Geochemical evidence from Neoproterozoic granitoids in South China. Lithos 113:347–368. https://www.nature.com/articles/nature08518#supplementary-information